

Report

R-24-06

December 2024



Corrosion of copper in unsaturated bentonite clay as a function of oxygen consumption

Haydn Haynes

Shorubhi Uthayakumaran

Andy Rance

Bharti Reddy

James Hesketh

SVENSK KÄRNBRÄNSLEHANTERING AB

SWEDISH NUCLEAR FUEL
AND WASTE MANAGEMENT CO

Box 3091, SE-169 03 Solna
Phone +46 8 459 84 00
skb.se

SVENSK KÄRNBRÄNSLEHANTERING

ISSN 1402-3091

SKB R-24-06

ID 2041836

December 2024

Corrosion of copper in unsaturated bentonite clay as a function of oxygen consumption

Haydn Haynes, Shorubhi Uthayakumaran, Andy Rance,
Bharti Reddy, James Hesketh

Amentum Clean Energy Limited

This report concerns a study which was conducted for Svensk Kärnbränslehantering AB (SKB). The conclusions and viewpoints presented in the report are those of the authors. SKB may draw modified conclusions, based on additional literature sources and/or expert opinions.

This report is published on www.skb.se

© 2024 Svensk Kärnbränslehantering AB

Executive summary

In order to safely dispose of spent nuclear fuel SKB has proposed placing the fuel in copper canisters. The copper canisters will be inserted into an underground repository that uses compacted bentonite as a buffer material. SKB has completed a number of in situ experiments to evaluate canister performance, but further experimentation is required to increase confidence in the behaviour of copper under anticipated repository conditions. One topic of experimentation is the performance of the copper canister in the early oxic period of an underground repository when the bentonite is partially saturated. Amentum proposed that such conditions could be simulated in lab-scale experiments through the use of bespoke glass cells. Key to the functionality of the glass cells is the use of oxygen sensor spots that monitor the in situ oxygen concentration without disturbing the internal conditions of the cell. This report discusses the trialling of this oxygen sensing method, and the results from a limited set of analyses used to inform how the copper is corroding under oxic conditions and in the transition to anoxic conditions.

OFP copper coupons were embedded in bentonite with a dry density of 1.45 Mg m^{-3} inside a stainless steel filter and sample holder. The glass cells were maintained in a $50 \text{ }^\circ\text{C}$ oven for a minimum of 249 days. Three glass cells were sacrificed after 251 days so that the coupons could be analysed using mass loss, XPS and Raman spectroscopy. A further two glass cells were dismantled after 621 days to enable further mass loss measurements to be performed. The key findings of the analyses were as follows:

- Oxygen was consumed in the test cells at different rates over the test duration. Contrary to initial expectations, the major cause of oxygen consumption was via corrosion of the base of the stainless steel sample holders, which was generated, or at least exacerbated, by the leaching of acetic acid from a silicone rubber compound used in the cells. In addition to that, during the course of the experiment, several test cells were accidentally tipped over, leading to corrosion of the internal stainless steel filters, which resulted in rapid depletion of oxygen in the cells. For cells that tipped over, contamination by salt water influenced the test environment for the copper coupons and meant that the test was no longer valid.
- Two large cells were sacrificed after 251 days, at which point their oxygen concentrations had reduced to 7.5 % and 16.5 %. A higher average corrosion rate, of $0.23 \text{ } \mu\text{m yr}^{-1}$ compared to $0.10 \text{ } \mu\text{m yr}^{-1}$, was observed in the cell that exhibited the lower oxygen concentration. The difference between these corrosion rates was not significant when the measurement uncertainty was considered. These results show that above a final oxygen concentration of 7.5 % a reduction in oxygen concentration due to consumption by corrosion of the stainless steel sample holder did not lead to a reduction in the corrosion rate of the copper coupons in these cells.
- Two medium cells were sacrificed after 621 days, at which point their oxygen concentrations were 7.4 % and 0 %, with the 0 % cell having turned anoxic after 209 days of exposure. The cell that had turned anoxic exhibited a lower average corrosion rate than the cell containing residual oxygen ($0.04 \text{ } \mu\text{m yr}^{-1}$ compared to $0.06 \text{ } \mu\text{m yr}^{-1}$), which is consistent with a reduction in the corrosion rate of the copper coupons upon complete consumption of the oxygen within the cell by corrosion of the stainless steel sample holder. However, as above when measurement uncertainty is considered the results are not statistically significant. Therefore, the results could partly be attributed to random variation. The analysis considered eight corrosion coupons, and the significance of the finding could be improved by analysing more repeats.
- The corrosion products that formed on the copper coupons in the intact cells were consistent with the presence of the Cu(I) oxide cuprite (Cu_2O), and a minor amount of the Cu(II) hydroxide spertiniite ($\text{Cu}(\text{OH})_2$). The predominance of Cu(I) oxides indicates the full oxidation of the copper to Cu(II) was constrained during the experiment. This could suggest that the availability of oxygen at the coupon surfaces was limited by the presence of bentonite surrounding them. No copper sulphides were detected on any of the intact cell coupons analysed, but trace amounts of sulphide were associated with adhered bentonite. Copper sulphides were identified in the tipped cell and were tentatively attributed to the copper iron sulphide mineral bornite.
- In general, average corrosion rates for copper coupons were lower than anticipated across the set of experiments and were comparable to those expected during atmospheric corrosion in mild

conditions. This may be attributable to the low moisture content in the bentonite, of 8.2–13.5 % because of the selected RH of 75 %. The bentonite remained “dry” and powdery.

Overall, the trial indicated several unexpected occurrences that may warrant further investigation. These occurrences, along with recommended mitigation steps, are described below:

- In the current setup, the ability to measure the in situ corrosion rate of the copper coupons in bentonite in oxic, humid conditions as a function of the concentration of oxygen was prevented by the corrosion of the stainless steel components. Corrosion of the stainless steel was accelerated by the leaching of acetic acid from a silicone rubber compound used in the experimental configuration. Acetic acid leaching could be minimised by pre-curing the rubber compound or using a different compound all together. However, the presence of the stainless steel in its current geometry (filter) may still lead to some consumption of oxygen, owing to its comparatively high surface area. We therefore recommend adopting a configuration where the bentonite and copper coupons are housed in an open topped glass/PTFE holder i.e., all metal other than the corrosion test specimens is eliminated completely.
- As discussed above, the observed corrosion rates/products suggest that the availability of oxygen at the coupon interface may be reduced by the presence of bentonite. Further work is required to understand the consumption of oxygen by copper and bentonite independent of each other. Additionally, a beaker-like vessel could be used to limit the diffusion of oxygen to a single direction. By evaluating different bentonite thicknesses it could be possible to determine the extent to which bentonite limits the availability of oxygen at the coupon interface.
- The volume of oxygen in the current configuration is too large to be consumed by the corrosion of the copper over a suitable period (6 months to a year). For future testing, optimisation of the ratio of the headspace volume to the surface area of the copper could be achieved based on the results from the present study to ensure that oxygen consumption via corrosion occurs over the desired timeframe. This would then enable the oxic corrosion rate to be determined in-situ via the rate of depletion of oxygen, if validated with periodic mass loss measurements.
- The use of saturated salt solutions to maintain the humidity in the experimental cells introduces the risk of contaminating the bentonite and copper with hyper-saline solutions. Such contamination events make the experimental results unusable. This risk could be mitigated by using cells with a wider base that are less susceptible to tipping, as well as using cell holders to complete oxygen sensor measurements.
- Sealing the glass cells using glass blowing reduces the oxygen content inside the cell due to combustion and leads to a reduction in the initial oxygen concentration as well as discrepancies in the starting oxygen concentration between individual cells. We recommend sealing the glass using an epoxy resin in future testing to ensure the starting oxygen concentration is equal to the atmospheric partial pressure of O₂.

Contents

1	Introduction	9
1.1	Background	9
1.2	Aims and objectives	10
2	Methodology	11
2.1	Overview	11
2.2	Experimental matrix	12
2.2.1	Specimen preparation and cell assembly	13
2.3	Oxygen sensor measurement	13
2.4	Cell disassembly and post-test analysis	16
2.4.1	Overview	16
2.4.2	pH measurements	17
2.4.3	Moisture content of bentonite	17
2.4.4	Coupon mass loss	17
2.4.5	XPS of coupon corrosion products	18
2.4.6	Raman spectroscopy of coupon corrosion products	18
3	Results	19
3.1	Oxygen concentration measurements	19
3.1.1	Small cells (0.20 L)	20
3.1.2	Medium cells (0.40 L)	20
3.1.3	Large cells (0.75 L)	21
3.1.4	Control cells (0.20 L)	21
3.1.5	Oxygen consumption	22
3.2	Oxygen depletion calculations	23
3.3	Cell disassembly	24
3.3.1	Overview	24
3.3.2	Visual observations	24
3.3.3	Analysis of bentonite samples	26
3.4	Analysis of coupons	27
3.4.1	Corrosion rate	27
3.4.2	XPS	30
3.4.3	Raman spectroscopy	34
4	Discussion	37
4.1	Comments on test methodology validation	37
4.2	Influence of oxygen on corrosion rate	39
4.3	Nature of corrosion product	40
4.4	Future work	41
5	Conclusions	43
	References	45
	Appendix A Additional information	47
	Appendix B Estimated uncertainty of corrosion rate measurements	53

Acronyms and abbreviations

ABM	Alternative buffer material
Cu-OFD	Oxygen-free phosphorus doped copper
EDM	Electrical discharge machining
EDX	Energy dispersive X-ray analysis
FEBEX	Full-scale Engineered Barriers Experiment
LOT	Long Term Test of Buffer Material
PR	Prototype repository
RH	Relative humidity
SEM	Scanning electron microscope
SRB	Sulphate reducing bacteria
SSM	Swedish Radiation Safety Authority
XPS	X-ray photoelectron spectroscopy

1 Introduction

1.1 Background

SKB's disposal concept for spent nuclear fuel involves placing the fuel in copper canisters with a cast iron insert. The copper canisters will be emplaced in an underground repository surrounded by compacted bentonite. The copper canisters are expected to remain tight and contain the radioactive material for hundreds of thousands of years and therefore it is important to consider their corrosion behaviour over very long timescales.

Over the years, SKB has performed several in situ experiments which provide insight into the performance of the canister and bentonite buffer during emplacement in an underground repository. These experiments include, for example:

- Prototype repository (PR) (Taxén et al. 2012, Taxén 2013).
- Long Term Test of Buffer Material (LOT) experiment (Wersin 2013, Karnland et al. 2009, Karnland et al. 2011, Johansson et al. 2020).
- Alternative Buffer Material (ABM) experiment (Gordon et al. 2018).
- Miniature Canister (MiniCan) experiment (Smart and Rance 2009, Smart et al. 2012, 2013, Gordon et al. 2017, Aggarwal et al. 2015).
- Large scale gas injection test (Lasgit) (Wendel et al. 2022).

Of these in situ experiments, only the MiniCan experiment was configured with the specific goal of studying corrosion processes. The MiniCan experiment was set up in predominantly anoxic conditions, and the evolution of the environmental conditions was monitored over time. The other experiments listed above were conducted under initially aerobic conditions, and corrosion data was extractable from the analyses. The following conclusions have been drawn based on field tests (Johansson 2019):

- The depth of corrosion is, in general, greater in experiments in which larger bentonite volumes are installed. This is reasonable since the pore volume of the unsaturated bentonite contains air (residual oxygen).
- Large clay volume experiments (with greater residual oxygen contents), such as the previously mentioned SKB-led experiments (PR, Lasgit and LOT experiments) or experiments led by other waste management organisations (e.g., the Full-scale Engineered Barriers Experiment (FEBEX), conducted in Switzerland) produced divalent-copper, specifically oxygen-containing corrosion products e.g., di-copper chloride tri-hydroxide ($\text{Cu}_2(\text{OH})_3\text{Cl}$).
- In experiments with smaller amounts of residual oxygen, such as the MiniCan experiments, only monovalent copper oxide (Cu_2O) was observed. This coincided with the depletion of oxygen in the experiment over a period of a few months.
- Raman spectroscopic investigations of the MiniCan experiments also indicated the formation of monovalent copper sulphide (Cu_2S). Similarly, in the intermediate size LOT experiments, small amounts of sulphur-rich particles were detected. These observations are in contrast with: i) the large-scale PR experiment, where only trace amounts of sulphur were found; and ii) FEBEX, where no sulphur was detected on the copper specimens.
- When measured (not systematically), corrosion depths determined by mass-loss correlated well with both the amount of residual oxygen and temperature expected to be present in the experiment. This would indicate that the corrosion of copper under repository-like initial conditions is controlled by residual oxygen and temperature. It is probable that this finding is biased by the use of higher temperatures for larger experiments. As an example, copper coupons from LOT S2 and A3 show little variation in corrosion depth between 25 to 55 °C (Johansson et al. 2020).

The conceptual corrosion model used in SKB's safety assessments suggest that the amount of corrosion during the early (oxic) post-closure period is controlled by the availability and transport of oxygen, while the subsequent long-term corrosion rate is controlled by sulphide transport limitations (i.e., the groundwater sulphide concentration, and its diffusion through the bentonite buffer). Although this conceptual corrosion model is in qualitative agreement with the findings in the field experiments listed above, detailed interpretation of the experiments is difficult due to lacking information on the development of redox conditions during the experiments (except MiniCan). Also, due to the evaluation of corrosion by (integrated) mass-loss only after retrieval of the experiments, it is not known how the corrosion mechanism and rate develops over time in these tests.

The specific aims of the work presented in this report are as follows:

- Track the development of corrosion products on SKB-grade copper coupons (amounts and composition) as oxygen is consumed.
- Evaluate how the corrosion rate of copper develops with time as oxygen is depleted, via mass loss measurements.
- Ascertain whether mass loss and corrosion depth do or do not continue to increase after complete oxygen depletion.

1.2 Aims and objectives

The aim of the programme of work presented in this document is to design, setup and demonstrate the successful use of an appropriate experimental setup for tracking in situ oxygen concentrations in sealed experimental systems (with a focus on copper embedded in bentonite) and establish appropriate experimental parameters for tracking oxygen consumption over a suitable timeframe (~3–6 months). Prior to setting up the experiment the oxygen sensor spots were tested and verified against a calibrated oxygen meter.

The contents of this report focus on the trial of the sacrificial glass cells. To identify a suitable experimental matrix, it is essential to track the timescales for oxygen depletion in the conditions of interest. This will enable us to identify suitable time intervals for gravimetric analysis (mass loss) and, as a result, study the corrosion rate and formation of the corrosion product in relation to oxygen depletion over time.

2 Methodology

2.1 Overview

The experimental design involved exposure of copper coupons to MX-80 bentonite at a controlled temperature (50 °C) and relative humidity (75 % RH) inside sealed glass cells containing a finite amount of air/oxygen. The conditions were chosen to provide a high relative humidity, and elevated temperature. As discussed later, the measurement range of the oxygen spots was 0 to 50 °C (Table 2-3). To prevent damage to the oxygen spots, it was decided that the experimental temperature should not exceed that range. The amount of oxygen in each glass cell was controlled by its volume and was varied within the experiment by use of three different cells (0.20 L, 0.40 L and 0.75 L). Throughout the experiment, the concentration of oxygen in the headspace of each glass cell was measured periodically. The average corrosion rate of the copper coupons over the period of exposure was determined gravimetrically for selected cells, and surface analysis was performed on selected coupons to provide information on the composition of the corrosion products.

The cell design consists of a stainless steel sample holder and filter containing copper coupons embedded within bentonite sealed within a glass cell (Figure 2-1). Stainless steel was chosen for the sample holder and filter to prevent the movement of bentonite out of the experiment. The stainless steel would also resist the swelling pressure produced by the bentonite, but this is not expected to occur as the bentonite was equilibrated with a 75 % RH environment for 47 days prior to the experiment (Section 2.2.1). Under the experimental conditions (50 °C, 75 % RH) stainless steel is expected to be corrosion resistant (Figure 2-4 in King et al. (2016)). The stainless steel holder has holes on the sides and the top to allow the transport of oxygen and water vapour into the cell. Between the holes and the bentonite are two fluid permeable stainless steel filters, a circular filter on the top of the bentonite and a cylindrical filter surrounding the bentonite. Beneath the bentonite is the solid stainless steel base of the sample holder. The base of the glass cells contains a reservoir that was filled with a saturated sodium chloride salt solution to give a RH of ~75 % (Greenspan 1977). A silicone rubber lining was applied to the walls of the reservoir prior to adding the saturated salt solution to prevent salt from creeping up the walls of the reservoir. Figure 2-2 shows the configuration of a fully assembled glass cell containing a sample holder.

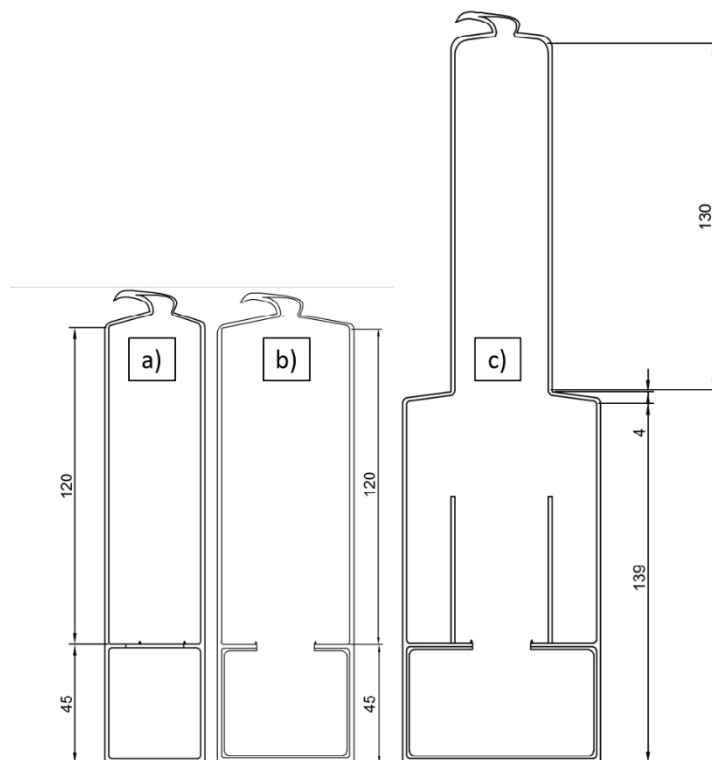


Figure 2-1. Diagram of the empty glass cells a) small (0.20 L), b) medium (0.40 L), c) large (0.75 L). Note the difference in scale between the large glass cell, and the small and medium glass cells.

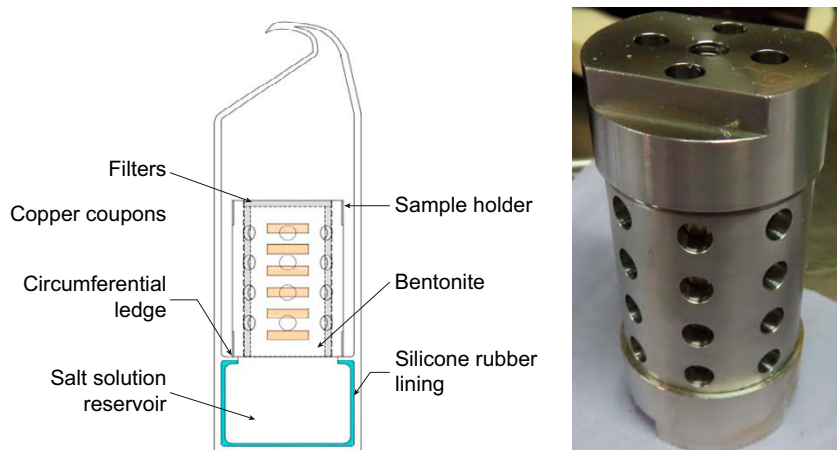


Figure 2.2. Diagram of a fully assembled small glass cell (left). The stainless steel sample holder is outlined. Inside the sample holder is a stainless steel filter highlighted in grey, the bentonite, and copper coupons (orange). The sample holder sits on a circumferential ledge that allows water vapour to disperse throughout the whole cell. A saturated salt solution sitting in the blue outlined reservoir humidifies the glass cell. A silicone rubber lining prevents salt creep from occurring. An image of the sample holder is shown on the right.

2.2 Experimental matrix

The experimental matrix is provided in Table 2-1. Experimental cells of a specific volume were assembled in triplicate and each contained a stainless steel sample holder, a stainless steel filter, six copper coupons, and an equal mass of MX-80 bentonite with a dry density of 1.45 Mg m^{-3} . Control cells were used to:

- Measure the consumption of oxygen within the cells by processes other than copper corrosion.
- Measure the extent of corrosion that takes place between emplacement of the copper coupons in the bentonite and sealing of the glass cells.

The control cells containing bentonite with no copper coupons were setup in triplicate and consisted of bentonite encased in a stainless steel sample holder and filter. The control cell containing only a stainless steel holder with no bentonite consisted of a single cell containing a stainless steel sample holder and its accompanying filter. A time zero control cell (t_0) was also prepared, which consisted of an assembled stainless steel sample holder containing bentonite and six copper coupons. The t_0 sample holder was not placed in a glass cell and was disassembled in an argon glovebox immediately after the rest of the glass cells had been sealed. The t_0 copper coupons were removed from the bentonite and stored in an argon atmosphere until analysis with the glass cells disassembled after 251 days.

Table A-5 in the appendix provides a full breakdown of the glass cells including cells that were disassembled for analysis, and cells that were accidentally tipped during the programme.

Table 2-1. Test matrix for the glass cells. t_0 refers to a cell that was setup and then immediately dismantled upon commencement of the experiment. Cells containing bentonite had a bentonite dry density of 1.45 Mg m^{-3} .

Cell type	Environment	Air volumes	Number of cells	Cell name
Experimental cells	6 × Copper coupons + bentonite (S#, M#, L#)	Volume 1 ~ 0.20 L (S#)	3	S#
		Volume 2 ~ 0.40 L (M#)	3	M#
		Volume 3 ~ 0.75 L (L#)	3	L#
Control cells	Bentonite (no copper coupons) (C#)	Volume 1 ~ 0.20 L	3	C#
	Stainless steel holder only (no bentonite) (SS)	Volume 1 ~ 0.20 L	1	SS
	6 × Copper coupons + bentonite (t_0)	N/A	1	t_0

2.2.1 Specimen preparation and cell assembly

Oxygen-free phosphorus doped copper (Cu-OFP) (Andersson-Östling et al. 2018) was provided by SKB in the form of blocks. The blocks of Cu-OFP were cut into cylindrical coupons with a diameter of 12 mm and a thickness of 3 mm using wire-cut electrical discharge machining (EDM). After cutting, the coupons were pickled in 5 % citric acid for 5 minutes. Following pickling the coupons were degreased by sonication in methanol for 5 minutes, vacuum dried, and stored in an argon atmosphere until use. All coupons were weighed three times and photographed before assembly in the sample holders.

Bentonite was weighed out for each sample holder targeting a bentonite dry density of 1.45 Mg m^{-3} . For the sample holders containing copper coupons the dry bentonite mass was 21.1 g, and for control cells with no coupons was 25.2 g (based on an initial water content of 5.8 wt.%). The bentonite was prepared in individual layers with an allowance made for the volume occupied by the coupons. The bentonite layers were prepared in small pots and exposed in a sealed container to a 75 % RH environment produced by a saturated sodium chloride solution for 47 days. Following pre-saturation the water content of the bentonite was $10.0 \pm 0.9 \text{ wt.}\%$. The humidified bentonite was poured into the stainless steel sample holders in seven layers. Each of the layers was compacted to the correct volume after each pour. A copper coupon was placed on top of each layer, except for the final layer which was used to fill the remaining volume left in the sample holder.

A silicone rubber layer was added to the inner surface of the reservoir located at the base of the glass cells. The glass cells were rotated to ensure even coverage of the compound and it was left to set. The required volume of sodium chloride was poured into the silicone rubber-lined well of the glass cells using a funnel. To preclude the possibility of microbial contamination of the reservoir water, deionised water was sterilised using an autoclave ($121 \text{ }^\circ\text{C}$, 20 mins). The sterile water was added to the salt in the reservoir using a funnel immediately before placing the stainless steel sample holders into the glass cells. The volume of deionised water used was equivalent to a third of the total volume of the well, specific volumes are provided in Table 2-2. The glass cells were sealed in air by a specialist glass blower (ASO Glassblowing Ltd, Wantage) on the 4th of November 2021. Once sealed, the glass cells were immediately transported back to Amentum's Harwell laboratories where they were placed in an oven at $50 \text{ }^\circ\text{C}$.

Table 2-2. Amounts of sodium chloride solution in the well of the glass cells.

Glass cell size (volume)	Mass of sodium chloride (g)	Volume of water (mL)
Small (~0.20 L)	10	15
Medium (~0.40 L)	20	29
Large (~0.75 L)	40	61

2.3 Oxygen sensor measurement

Measurement of the gas phase oxygen concentration was achieved using remote sensing spots. Oxygen concentration refers to the concentration of oxygen in the gas phase throughout the report and is proportional to the partial pressure. The sensor spots allow for the determination of the oxygen concentration through transparent materials i.e., glass (Figure 2-3). This enables measurement of the oxygen concentration in glass vessels without opening them. The sensors manufactured by Presens (Regensburg, Germany) react with oxygen and, in doing so, limit the fluorescence lifetime of an excited dye molecule (Liesch et al. 2000). The greater the oxygen concentration, the shorter the lifetime of the excited molecule (Figure 2-4). The dye molecule is initially excited by light produced by a fibre optic cable connected to the measurement device (Presens, Fibox 3 LCD trace). Collisions between the dye molecules (luminophores) and the quencher (in this case oxygen) cause radiationless deactivation known as dynamic quenching. Following collision the dye molecules do not emit luminescence and the measurable luminescence signal from the sensor spots decreases.



Figure 2-3. Close up image of one of the glass cells showing the location of an oxygen sensing spot (pink). The spot is attached to the inside of the glass using silicone rubber.

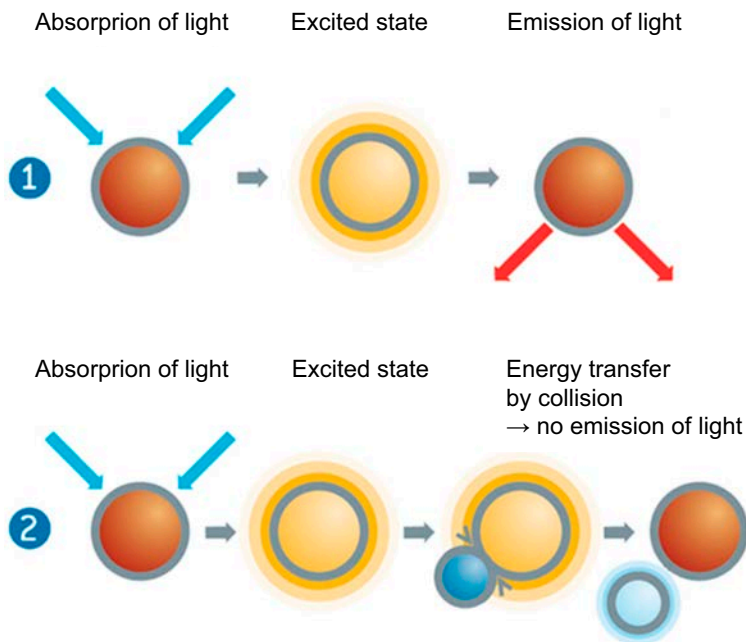


Figure 2-4. Diagram explaining how the Presens (Regensburg, Germany) oxygen sensors work adapted from PreSens (2024). 1. Luminescence process in the absence of oxygen leading to the emission of light. 2. Deactivation of the luminescent indicator molecule by molecular oxygen.

The sensor spots come in several varieties for use in different environments. For this work we chose the PSt3, and PSt6 range of sensor spots, which are designed to measure between 0 to 100 %, and 0 to 5 % oxygen concentration respectively. A more detailed breakdown of their technical specification is shown in Table 2-3.

Table 2-3. Specifications of the oxygen sensor spots chosen for the trial. PSt3 and PSt6 are the product names provided by the manufacturer.

Specification	PSt3	PSt6
Measurement range (%)	0 to 100	0 to 5
Limit of detection (%)	0.03	0.002
Resolution (%)	± 0.01 at 0.21 ± 0.1 at 20.9	± 0.0007 at 0.002 ± 0.0015 at 0.2
Accuracy	± 0.4 at 20.9 % ± 0.005 at 0.2 %	± 1 ppb or ± 3 % of the respective concentration whichever is higher
Measurement temperature range (°C)	0 to 50	
No cross-sensitivity	pH 1–14, CO ₂ , H ₂ S, SO ₂ , ionic species	
Cross sensitivity	organic solvents, chlorine gas	

Pre-determined calibration constants for the individual oxygen sensor spot batch were provided by the manufacturer. These constants were programmed into the measurement device before each set of measurements. Verification of the sensor spots was completed during the initial tests and the results are shown in Figure 2-5. The readings produced by the oxygen sensor spots were compared to a Systech oxygen meter in a closed system. The results from both the PSt6 (0 to 5 %) and the PSt3 (0 to 100 %) spots show that the readings can be fitted linearly with R^2 values of 0.9996, and 0.9993 respectively. Despite the high precision of the two techniques, as judged by the size of the error bars, the two techniques were not in complete agreement. In the case of the PSt6 (0 to 5 %) oxygen sensor spots the sensor spots had a value 19.7 % higher than the measured percentage on the Systech oxygen meter, excluding the result outside of the 5 % measurement range. The PSt3 (0 to 100 %) oxygen sensor spot oxygen saturation readings were 1.6 % lower than the measured percentage on the Systech oxygen meter. Several differences exist between the two sampling techniques that may explain the discrepancy observed between the measurements. For example, the oxygen sensor spots measure the concentration of oxygen in contact with the sensor spot, which is a small volume of the test vessel, while the Systech oxygen meter pumps the oxygen through an electrochemical cell which is a more representative sample of the whole system. The sampling times of the two techniques are also different with the oxygen sensor spots having a sampling time of less than 6 seconds, while the sampling time of the Systech oxygen meter is 30 seconds.

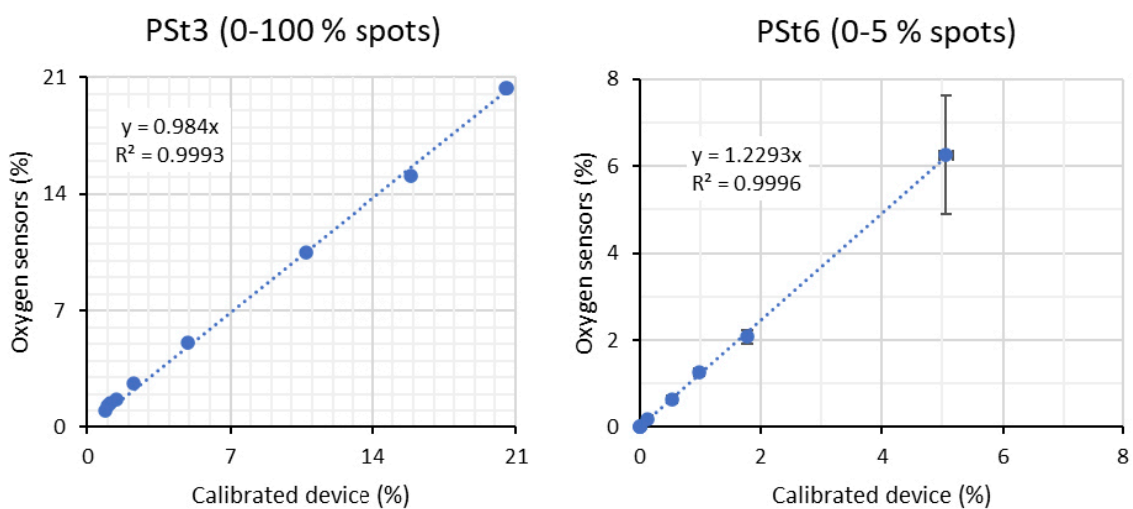


Figure 2-5. Comparison of the oxygen reading from the Presens oxygen sensor spots, compared to a calibrated Systech oxygen meter. PSt3 and PSt6 are the product names provided by the manufacturer.

To make oxygen measurements during the experiment, the glass cells were removed from the oven one at a time. The measurement of oxygen concentration via the sensor spots experiences a temperature dependence, so it was necessary to make measurements with the cells at the same temperature each time. To achieve this a temperature sensor was attached to the glass cell and the oxygen reading was taken when the temperature dropped to 26.9 °C (the highest temperature that could be replicated across all glass cell volumes). A single measurement was taken (multiple readings are not possible due to the continued cooling of the glass cell) and the process was repeated for all cells in a given measurement interval. Measurement intervals were approximately every week for the duration of the experiment (in this report 621 days).

2.4 Cell disassembly and post-test analysis

2.4.1 Overview

Cells were disassembled in an argon-purged glovebox by scoring the glass cell and fracturing them along the score line. Test specimens were removed from the bentonite, photographed and stored under argon in Mylar bags until they were analysed. Samples of bentonite were taken from each cell for analysis. Aliquots of the salt solution were also retained from selected cells¹ for chemical analysis.

After 251 days of operation three glass cells were chosen for dismantling (L1, L2, and S3). The decision on which cells to dismantle was made based on the measured oxygen concentration in each of the chosen cells.

- Cell S3 was anoxic almost from the start of the test, as a result of being tipped.
- Cell L1 was terminated with an oxygen concentration of 7.5 %.
- Cell L2 was terminated with oxygen concentration of 16.5 %.

This allowed the corrosion rate of the copper coupons to be assessed after comparable durations with a varying oxygen concentration. The cells that were disassembled are summarised in Table 2-4.

After 614 days a further two glass cells were dismantled (M1 and M3) to increase the confidence in the mass loss measurements.

- Cell M1 went anoxic after 209 days.
- Cell M3 was terminated after 614 days with an oxygen concentration of 7.4 %.

Comparison of cells M1 and M3 was used to infer whether corrosion occurred in Cell M1 after going anoxic at 209 days. This was based on the hypothesis that corrosion would cease in Cell M1 upon depletion of the oxygen, while corrosion would continue in the oxic environment of Cell M3.

Table 2-4. Matrix of glass cells. Cell nomenclature is highlighted in bold text.

Cell type	Environment	Air volumes of all cells	Number of cells set up	Cells disassembled	Cells remaining
Experimental Cells	6 × Copper coupons + bentonite (S# , M# , L#)	Volume 1 ~0.20 L (S#)	3	S3	S1 & S2
		Volume 2 ~0.40 L (M#)	3	M1 & M3	M2
		Volume 3 ~0.75 L (L#)	3	L1 & L2	L3
Control cells	Bentonite (no copper coupons) (C#) Stainless steel holder only (no bentonite) (SS) 6 × Copper coupons + bentonite (t₀)	Volume 1 ~0.20 L	3	-	C1, C2 & C3
		Volume 1 ~0.20 L	1	-	SS
		N/A	1	t ₀	-

¹ This was not part of the scheduled analysis plan but was performed as part of quality assurance after some cells exhibited corrosion on the external surface of the stainless steel sample holder.

2.4.2 pH measurements

The pH of the salt solutions and bentonite was measured using a Jenway 3510 pH meter. Immediately prior to use, the pH meter was calibrated using pH 4, pH 7 and pH 10 buffer solutions. The pH probe was washed with deionised water and dried before taking individual measurements. The salt solutions received no prior treatment. For the bentonite measurements a sample of 0.8 g bentonite was removed from the disassembled cell and added to a centrifuge tube containing 40 ml of deionised water. The mixture was left to equilibrate for 3 hours, and the pH was measured using the calibrated pH meter and a glass pH probe.

2.4.3 Moisture content of bentonite

An approximate moisture content of the bentonite in the stainless steel sample holders was determined after disassembly of the cells using a mass loss method. Approximately 1 g of bentonite was placed in an oven at 110 °C for 1 hour. The sample was then weighed, and the moisture content of the sample calculated according to Equation 2-1, where MC is moisture content, and m is the bentonite mass at different steps.

$$MC = \left(\frac{m_{wet} - m_{dry}}{m_{dry}} \right) \times 100 \quad \text{Equation 2-1}$$

2.4.4 Coupon mass loss

To calculate the average anaerobic corrosion rate of the coupons, mass loss measurements were carried out on each coupon in accordance with procedure ASTM G1-03 (ASTM 2017), as summarised below:

- Prior to assembly of the modules, all the specimens were weighed after degreasing them in methanol and drying for 10 minutes under vacuum to determine their initial mass (designated M_0).
- After exposure testing, the specimens were cleaned of residual bentonite by sonication in methanol for five minutes. Following sonication, the methanol was decanted, and the specimens were left to dry naturally in the glovebox for 10 minutes. The specimens were weighed to give the solvent mass (M_s)².
- The initial solvent cleaning procedure was followed by a chemical cleaning /descaling procedure which consisted of:
 1. Submerging the coupons in 18 % w/v hydrochloric acid (deaerated) for 2 minutes.
 2. Rinsing three times in deionised water.
 3. Sonicating for five minutes in deionised water.
 4. Sonicating for five minutes in methanol.
 5. Vacuum drying for five minutes.
 6. Reweighing reweighed (giving mass, M_1).
- To account for possible mass loss due to dissolution of metal during determination of M_1 , and assuming all corrosion products had been removed by descaling at this point, steps 1–6 were repeated four more times, giving mass M_2 , M_3 , M_4 and M_5 .

The mass loss calculations were carried out according to Section 8 of ASTM G1-03 (ASTM 2017). The change in coupon mass following each cleaning cycle (i.e., steps 1–5) was plotted. The y-intercept of a straight line fit through the data following the point at which the corrosion products had been fully removed by descaling (i.e., for mass changes determined after the 2nd–4th iterations of the full cleaning cycle³) was produced according to:

$$y = mx + c \quad \text{Equation 2-2}$$

² The solvent mass is recorded but does not serve a purpose in the corrosion calculations.

³ If the corrosion product persisted after the first cleaning cycle, then the y-intercept was found from data generated after the 3rd–4th iterations of the cleaning cycle etc.

Where,

- y is the change in the coupon mass following each of the cleaning steps,
- m is a fitting constant equivalent to the rate of metal loss within the cleaning solution,
- x is the cumulative time spent in the cleaning solution,
- c is the mass loss due to corrosion.

The mass loss, (c in Equation 2-2), was then converted to a corrosion rate given in units of $\mu\text{m yr}^{-1}$.

Details regarding the uncertainty associated with the mass loss measurements are provided in Appendix B.

2.4.5 XPS of coupon corrosion products

The surfaces of three corrosion coupons were analysed using X-ray photoelectron spectroscopy (XPS) and ion beam depth profiling, to determine the surface composition and the oxidation state of the predominant species. Samples were analysed using a Thermo Scientific K-Alpha XPS instrument equipped with a microfocussed monochromated Al X-ray source. The source was operated at 12 keV and a 400-micron radial spot size was used. The analyser operated at a constant analyser energy (CAE) 200 eV for wide survey scans and 50 eV for high resolution scans. Wide survey scans were used to determine elemental composition, including surface adventitious carbon. High resolution scans were collected to determine elemental chemical state information.

The data acquisition and analysis were performed with Thermo Scientific's Avantage software. Peak fitting (Lorentzian / Gaussian (L/G) 30 %) was applied following removal of a Smart background. Normalised atomic percentages were determined from peak areas of the elemental main peaks detected on the survey scan following background subtraction and application of 'Thermo' sensitivity factors. Depth profiling was achieved using 2 kV Ar^+ ions at the medium current setting which is equivalent to an erosion rate of ~ 1 nm per minute. Profiles were obtained in 15 steps with 20 s ion bombardment per step for a total of 300 s etching. Each sample was analysed in three positions and depth profiled in one. Both wide binding energy and detailed scans were undertaken after each depth profiling step.

2.4.6 Raman spectroscopy of coupon corrosion products

Raman spectroscopy was used to analyse the corrosion product, using a Horiba JY LabRam Aramis confocal Raman microscope. The exciting laser wavelength used was 532 nm. A $\times 50$ extra-long working distance objective lens was used to collect the 180° backscattered light. The specimens were loaded into sample holders subsequently used for Raman measurements inside an argon-purged glovebox and held in place using Menzel Gläser cover slips attached to the sample holders using Araldite® adhesive. This ensured that the specimens were not exposed to air before or during the analyses.

All Raman spectra were processed post-data collection to remove the baseline which arises from background fluorescence and/or Rayleigh scattering. In particular, the fluorescence from residual bentonite is the major contributor to the background signal. The background of each spectrum was computed by one of two main methods: asymmetric least squares (Peng et al. 2010) and iterative reweighted quantile regression (Han et al. 2018).

3 Results

3.1 Oxygen concentration measurements

The oxygen concentration in the headspace of the glass cells was measured using oxygen sensor spots as described in Section 2.3. Measurements were completed every week except for an interval between day 41 and 67 due to seasonal holidays. The first 621 days of oxygen measurements including the dismantling of S3, L1 and L2 (251 days) and M1 and M3 (614 days) are described in Sections 3.1.1 to 3.1.4. Oxygen measurements were halted at day 621, but the remaining glass cells continue to operate under the experimental conditions (sealed, 50 °C).

Following installation of the cells in the oven, three of the glass cells (C1, M2, S3) tipped over after day 1 (Table 3-1). This occurred due to vibrations in the oven when no staff were present and had not been observed with the previous trials. Additionally, a further glass cell (S2) was tipped over during measurement on day 96 because of user error (Table 3-1). The consequence of the cells tipping over was that the saturated sodium chloride solution that was used to control the cell humidity leaked from the reservoir at the base of the ampoule and made contact with the stainless steel sample holder, contaminating part of the bentonite with saltwater. In cells where this occurred, the oxygen in the cell decreased rapidly as it was consumed by rapid corrosion of the stainless steel filter due to contact with the saturated sodium chloride solution.

Initial attempts to measure the oxygen concentration were hampered by differences in the cooling of the cells upon removal from the oven, since the measurement exhibits a temperature dependence. This was mitigated from day four onwards by measuring the oxygen concentrations after the glass cells had cooled to a target temperature of 26.9 °C. Consequently, the measurement data gathered prior to this (i.e., the first four days) is not comparable and has been omitted. In addition, the glass cells were flame-sealed which resulted in consumption of some of the oxygen in the cells. As a result, the initial oxygen concentration in each of the cells at the start of the experiment was lower than 21 %. Further discussion of the discrepancies observed in the rate of oxygen consumption between individual glass cells is described in Section 4.1.

Table 3-1. Summary of cells that tipped over during operation. Cell nomenclature is highlighted in bold text.

	Environment	Air volumes	Cells tipped
Experimental cells	6 × Copper coupons + bentonite (S# , M# , L#)	Volume 1 ~0.20 L (S#) Volume 2 ~0.40 L (M#) Volume 3 ~0.75 L (L#)	S2 & S3 M2 -
Control cells	Bentonite (no copper coupons) (C#) Stainless steel holder only (no bentonite) (SS) 6 × Copper coupons + bentonite (t₀)	Volume 1 ~0.20 L Volume 1 ~0.20 L N/A	C1 - N/A

3.1.1 Small cells (0.20 L)

The oxygen concentrations in the small cells over 621 days are shown in Figure 3-1. Following the tipping of Cell S3 at the start of the experiment, its oxygen concentration decreased sharply, becoming fully depleted by day 12. The oxygen concentration in Cell S3 remained depleted until dismantling on day 251. Compared to Cell S3, the oxygen concentration of cells S1 and S2 decreased more slowly. Cell S2 decreased from 18.4 % on day 4 to 11.1 % by day 96. Tipping of Cell S2 on day 96 was followed by an increase in the rate of oxygen consumption, with Cell S2 becoming anoxic by day 158. The oxygen concentration in Cell S1 decreased in a smooth trend, starting at 17.6 % on day 4 and reaching depletion by day 182. After depletion the oxygen concentration in Cells S1 and S2 remained anoxic until day 621.

3.1.2 Medium cells (0.40 L)

The oxygen concentration of the medium cells over 621 days is shown in Figure 3-2. Cell M2 was tipped at the start of the experiment and became anoxic by day 21 and remained depleted until day 621. The consumption of oxygen in Cell M1 was fairly linear with an oxygen concentration of 16.5 % on day 4 and reaching depletion by day 209. Cell M3 remained oxidic over the reported period with the oxygen concentration decreasing from 16.3 % on day 4 to 7.4 % on day 607. Cells M1 and M3 were dismantled on day 614.

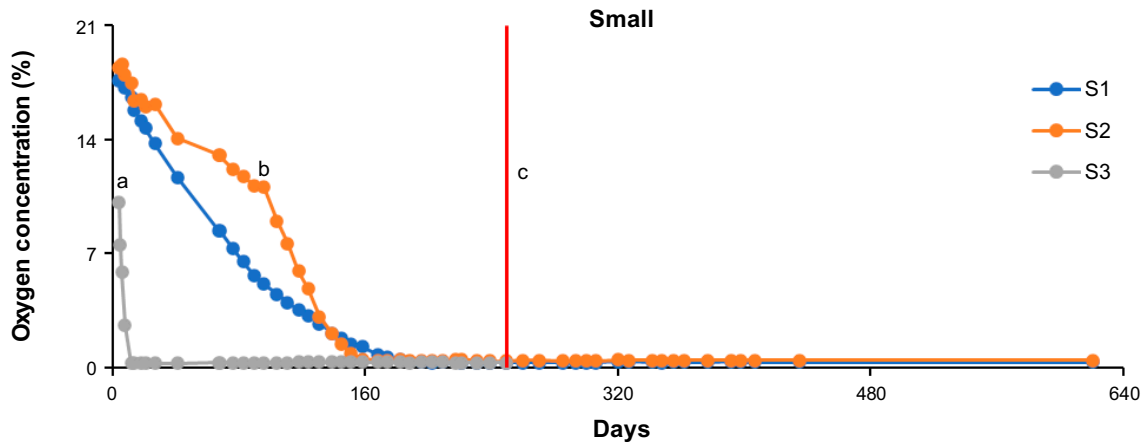


Figure 3-1. Oxygen concentration in the small cells (S#) over the initial 621 days of the experiment. ^aCell S3 was tipped at the start of the experiment. ^bCell S2 was tipped after 96 days. ^cCell S3 was dismantled after 251 days. Glass cells were operated at 50 °C.

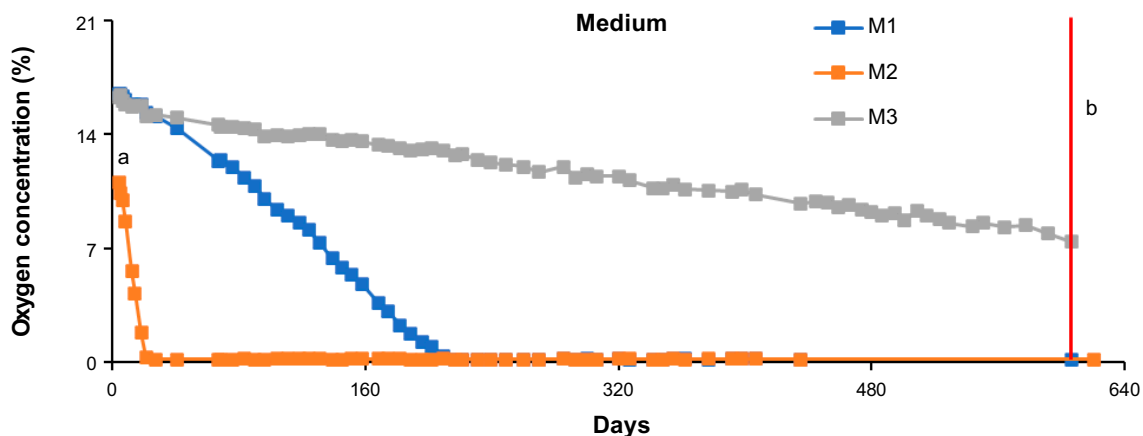


Figure 3-2. Oxygen concentration in the medium cells (M#) over the initial 621 days of the experiment. ^aCell M2 was tipped at the start of the experiment. ^bCells M1 and M3 were dismantled after 614 days. Glass cells were operated at 50 °C.

3.1.3 Large cells (0.75 L)

The oxygen concentration of the large cells over 621 days are shown in Figure 3-3. Cells L2 and L3 showed similar trends, but with different initial oxygen concentrations. Cell L2 decreased from 19.2 % on day 4 to 16.5 % on day 249, while Cell L3 decreased from 13.4 % on day 4 to 5.4 % on day 621. Cell L2 was dismantled on day 249. The oxygen consumption in Cell L1 was also linear between day 4 and day 196, decreasing from 16.7 % to 13.0 %. However, after day 196 there was an inflexion in the rate of oxygen consumption and by day 249 the oxygen concentration in Cell L1 had decreased to 7.5 %. Cell L1 was dismantled on day 249.

3.1.4 Control cells (0.20 L)

The oxygen concentrations of the control cells over 621 days are shown in Figure 3-4. Cell C1 was tipped at the beginning of the experiment, and its oxygen concentration was depleted by day 6. The oxygen concentration in Cells C2 and SS decreased in a smooth continuous trend, with Cell C2 decreasing from 18.1 % on day 4 to depletion by day 145, and Cell SS decreased from 20.4 % on day 4 to depletion on day 342. The oxygen concentration in Cell C3 decreased at the slowest rate from 17.9 % on day 4 to depletion on day 435. After oxygen depletion all the control cells remained anoxic until day 621.

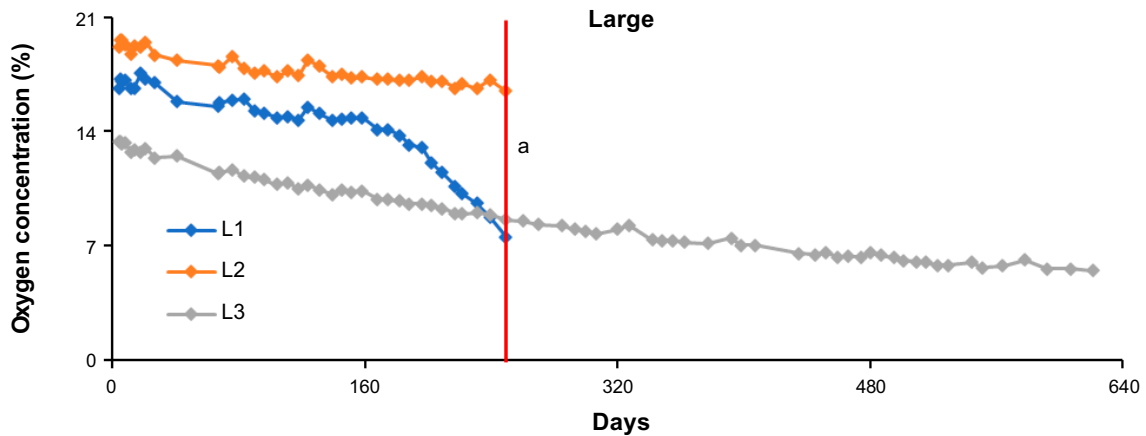


Figure 3-3. Oxygen concentration in the large cells (L#) over the initial 621 days of the experiment. ^aCells L1 and L2 were dismantled after 251 days. Glass cells were operated at 50 °C.

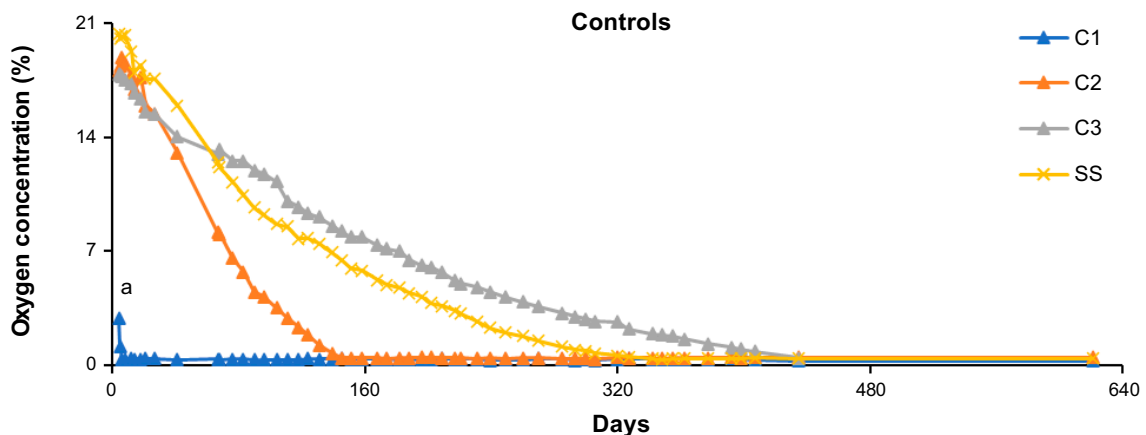


Figure 3-4. Oxygen concentration in the bentonite + sample holder control cells (C#) and the sample holder only control cell (SS) over the initial 621 days of the experiment. ^aCell C1 was tipped at the start of the experiment. Glass cells were operated at 50 °C.

3.1.5 Oxygen consumption

The amount of oxygen consumed in each set of glass cells was compared to determine if there was a difference between different cell volumes and the controls (Figure 3-5). Note that the control cells had the same size as small cells, thus comparisons between those cells are more appropriate than comparisons between control cells and medium or large cells.

The amount of oxygen consumed was compared between day 4 and day 158, as this period provided the most datapoints where the oxygen consumption was steady. Tipped cells were excluded from the interpretation due to the measurements being influenced by the saturated sodium chloride solution. The amount of oxygen consumed over the 154 day period in each glass cell was approximately 0.69 mM. The greatest standard deviation in the oxygen consumption rates was observed in the medium cells (± 0.70 mM), and bentonite and sample holder controls (± 0.29 mM), which comprised two functioning tests (i.e., those that had not been tipped over). The large cells exhibited the lowest standard deviation (± 0.15 mM) from measurements taken from three functional tests. Standard deviations of the small cells and stainless steel only control test were not reported as only one functional cell was available from each.

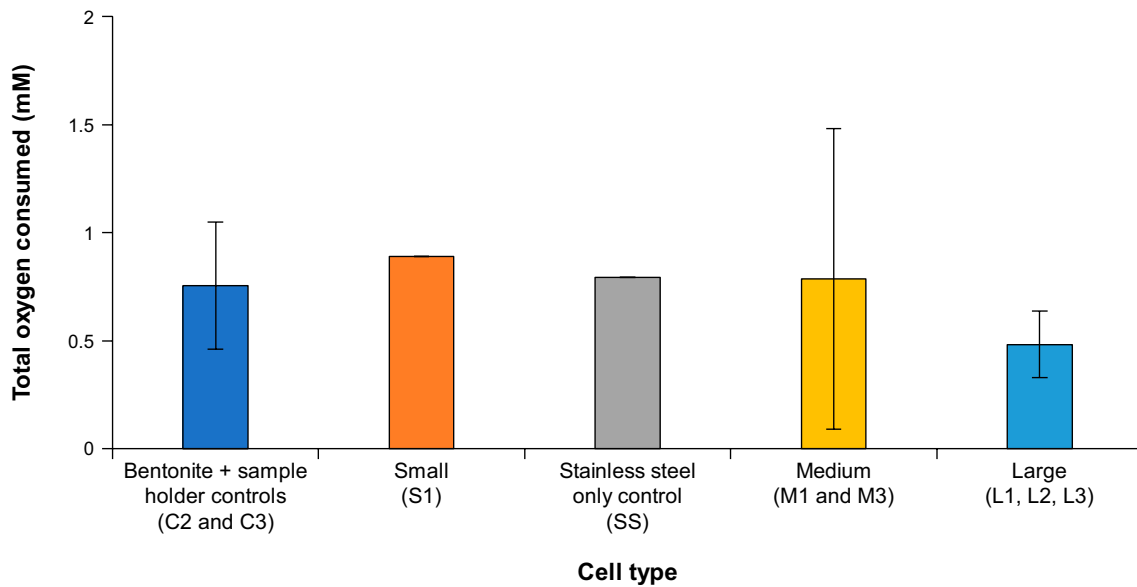


Figure 3-5. Comparison of the total amount of oxygen consumed in the glass cells between day 4 and day 158. Small, medium and large cells contained 22.3 g of bentonite. Bentonite and sample holder control cells contained 26.6 g of bentonite (note that control cells have the same volume as the small cells). Tipped cells were excluded from the comparison.

3.2 Oxygen depletion calculations

To support interpretation of the oxygen depletion measurements, an equivalent oxygen consumption rate by copper corrosion was determined using the average mass loss value from Cell L2 of $0.1 \mu\text{m yr}^{-1}$ (Table 3-6). This corrosion rate was used to estimate the rate of consumption of oxygen in the different cell volumes by considering the uniform formation of CuO (i.e., 1 mol of O_2 oxidised 2 mol of Cu to Cu^{2+}) on the surface area of the 6 coupons. It was assumed that the initial amount of oxygen present in each cell was equivalent to that calculated by the ideal gas law calculated for air at standard temperature and pressure, and that the corrosion rate was independent of the oxygen concentration (i.e., persisted at the initial assumed rate of $0.1 \mu\text{m yr}^{-1}$).

The estimated rate of depletion and time to depletion of oxygen in each of the three cell volumes (small, medium and large) based on the assumed corrosion rate of $0.1 \mu\text{m yr}^{-1}$ is shown in Figure 3-6. The estimated time to depletion of the small, medium and large cells based on the assumed corrosion rate is 54 years (19810 days), 108 years (39610 days) and 217 years (79210 days), respectively. These durations correspond to depletion rates of 0.4 \% yr^{-1} , 0.2 \% yr^{-1} and 0.01 \% yr^{-1} for different types of cells respectively. Hence, based on the durations of exposure reported in Section 3.1 (249 days), at a corrosion rate of $0.1 \mu\text{m yr}^{-1}$ the amount of oxygen consumed by copper corrosion would be of the order of 0.07 to 0.27 % depending on the cell volume. The amount of oxygen consumption in the glass cells far exceeded that expected by copper corrosion alone. Therefore, under the prevailing assumptions (specifically the corrosion rate measured for copper), it can be inferred that most of the oxygen depletion that was observed in all cells, both those that tipped and those that remained upright, was attributable to processes other than copper corrosion e.g., stainless steel corrosion and possibly also reactions with bentonite.

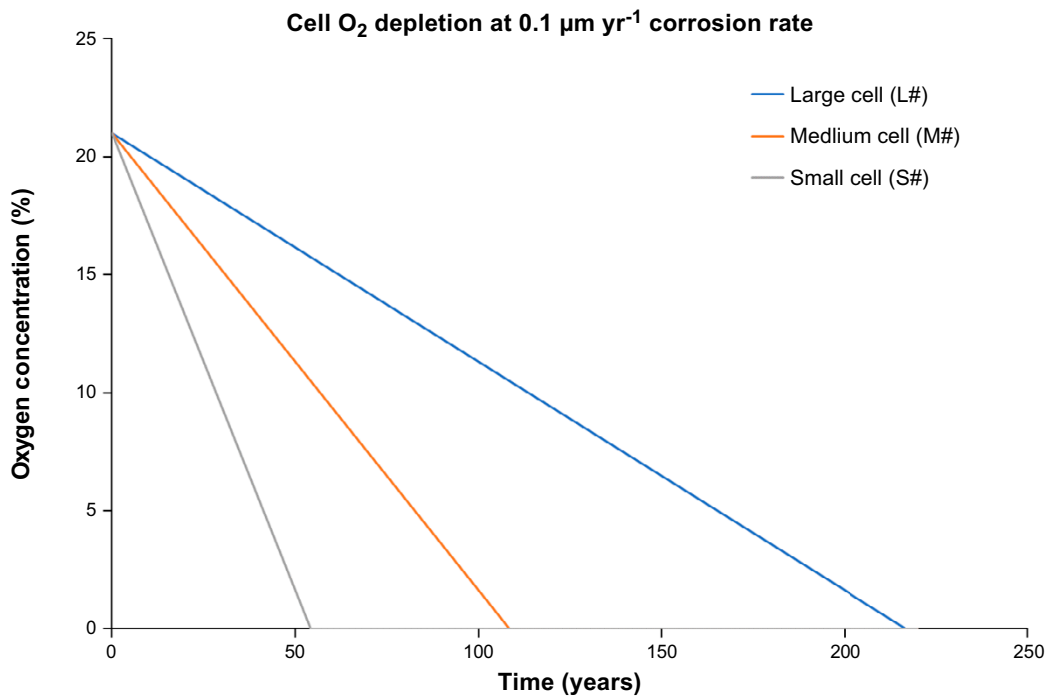


Figure 3-6. Estimated rate of depletion of different sized cells based on an assumed copper corrosion rate of $0.1 \mu\text{m yr}^{-1}$.

3.3 Cell disassembly

3.3.1 Overview

Following 251 days of testing, the decision was made to disassemble cells L1, L2 and S3. The rationale for selecting cell L1 and L2, was that the oxygen concentration in L1 had remained consistently lower than that of L2 for the duration of the exposure period and had also depleted at a higher rate. S3 was tipped on the first day leading to the rapid consumption of oxygen, and therefore would have acted as a cell that had been anoxic for almost all the exposure period (249 days). However, inspection of the cell revealed that the bentonite was contaminated with large amounts of iron corrosion products from the tipping event, so was not considered a valid test. Based on the calculations presented in Section 3.2, the oxygen depletion in the cells is likely to be dominated by processes other than copper corrosion (e.g., reactions with bentonite and reactions with the stainless steel). Hence, by comparing the copper specimens in L1 and L2, it is possible to evaluate whether the difference in oxygen concentration had a significant impact on the corrosion rate or the chemistry of the corrosion products.

Following the initial dismantling after 249 days, it was decided that a second dismantling stage would be beneficial to expand the mass loss dataset. After 614 days M1 and M3 were dismantled. Cell M3 was selected because it remained oxic throughout the experiment and had a similar oxygen concentration to Cell L1 at the end of the experiment. The other dismantled medium cell (M1) became anoxic on day 209 and therefore could be used to infer whether the depletion in oxygen that occurred after 209 days led to a reduction in the average corrosion rate by comparison against the corrosion rate of the coupons in cell M3. Table 3-2 shows the initial (measured at 4 days) and final oxygen concentration measured in each of the cells, and the average oxygen concentration in each of the cells approximated over the measurement duration by linear interpolation between measurement intervals.

Table 3-2. Summary of oxygen concentrations for disassembled experimental cells.

Designation	Volume (L)	Duration (Days)	Initial O ₂ (%) ⁴	Final O ₂ (%)	Average O ₂ (%) ⁴
L1	0.75	249	16.7	7.5	14.0
L2	0.75	249	19.2	16.5	17.4
S3	0.20	249	10.2	0 (Day 12) ⁵	0.4
M1	0.40	614	16.5	0 (Day 209) ⁵	3.2
M3	0.40	614	16.3	7.4	11.5

3.3.2 Visual observations

Photographs of the corrosion coupons were taken before sample holder preparation, and after exposure and removal from the glass cell. Table 3-3 provides representative images of the pristine and ‘as removed’ coupons (i.e., no treatment of the coupons before the photographs were taken). Key observations with respect to the bentonite and corrosion coupons are reported below,

- The bentonite on coupons from the tipped Cell S3 appeared to be moist owing to contamination with the salt water from the reservoir at the bottom of the ampoule (not shown). The bentonite on coupons from cells L1, L2, M1 and M3, which remained upright throughout the duration of exposure, was dry (not shown).
- All the coupons removed had bentonite adhered to their surface. The coupons from Cell S3 had a purple sheen to them, but the original copper colour was still visible in some areas. Coupons from the two large cells exposed for 249 days (L1 and L2) exhibited shiny patches of orange/red and separate regions of dull brown colour. The colouration of the coupons from the medium cells after exposure for 614 days (M1 and M3) was similar to the coupons from the large cells, but more tarnishing, as well as the presence of purple areas, was observed. Individual coupons from the same large and medium cells exhibited a variation in the extent of discolouration, with some appearing more corroded than others.

⁴ Not including the first 4 days of exposure.

⁵ Day the cell reached 0 % O₂.

Table 3-3. Images of the coupons used in S3 (0.20 L, 0 % end O₂, NaCl contaminated, 249 days), L1 (0.75 L, 7.5 % end O₂, 249 days), L2 (0.75 L, 16.5 % end O₂, 249 days), M1 (0.40 L, 0 % end O₂, 614 days) and M3 (0.40 L, 7.4 % end O₂, 614 days). (The coupon number designates the cell and the number of the specific coupon from that cell).

Coupon #	Pristine	Side A	Side B
S3-3			
L1-4			
L2-3			
M1-3			
M3-3			

3.3.3 Analysis of bentonite samples

The results of the pH measurements carried out in solutions equilibrated with the bentonite from dismantled cells are given in Table 3-4. A bentonite sample was not obtained from the tipped cell (S3), so all reported bentonite pH values were from non-tipped cells. All the measured bentonite solutions (0.8 g in 40 mL DI) gave approximate pH values of 10, which is at the limit for which the pH meter was calibrated. Where the pH is above 10 the pH response is anticipated to remain linear within this small extrapolation, so the measurements are considered valid.

Greater variability was observed in the saturated salt solutions located in the reservoir of the glass cells. The pH of the salt solution in cell M3 had a circumneutral pH (7.2), with cells M1, L2, and S3 having slightly acidic pH values (~5.7). The lowest pH was observed in cell L1 (2.8), which was below the lowest measurement range of the pH standards used to calibrate the meter (4). The deviation from the measurement range was large, and therefore the value for L1 should be considered an approximate value.

Table 3-4. pH of deionised water equilibrated with the bentonite samples (0.8 g in 40 mL), as well as the pH of the salt solution in the glass cell reservoirs. All pH values were determined after dismantling the glass cells.

Glass cell size (volume)	Cell identifier	Bentonite pH	Reservoir pH
Small (~0.20 L)	S3 (tipped)	*	6.2
Large (~0.75 L)	L1	10.1	2.8
	L2	10.1	5.5
Medium (~0.40 L)	M1	10.0	5.5
	M3	10.1	7.2

* pH of the bentonite from S3 was not determined. Cell S3 was tipped at the start of the experiment, while the other cells remained non-tipped for the duration of the experiments.

Results from the bentonite moisture content measurements are given in Table 3-5. The small cell that tipped over (S3) exhibited a higher bentonite moisture content (27.7 %) than the two large and two medium cells in which the bentonite remained comparatively dry. The bentonite moisture content in the two large cells (L1 and L2) and M1 were similar to each other (~12.8 %), with the bentonite moisture content in M3 being lower (8.2 %). Comparisons with experimentally derived water retention curves for MX-80 bentonite imply that for a temperature of 50 °C and 75 % RH the moisture content would be ~14 wt. % (Dueck and Nilsson 2010).

Table 3-5. Moisture content of bentonite samples taken from disassembled cells.

Glass cell size (volume)	Cell identifier	Average moisture content (wt. %)	Standard deviation of moisture content (wt. %)
Small (~0.20 L)	S3 (tipped)	27.7	1.0
Large (~0.75 L)	L1	12.0	0.7
	L2	12.8	0.6
Medium (~0.40 L)	M1	13.5	0.2
	M3	8.2	0.1

3.4 Analysis of coupons

3.4.1 Corrosion rate

The corrosion losses over the total exposure period were determined from the mass loss of four coupons taken from each of the disassembled cells according to the procedure described in Section 2.4.4. These measurements reflect the average corrosion thickness loss from the point when the coupons were in contact with the bentonite (including the brief period prior to the cells being sealed), until the experiments were dismantled. The extent of corrosion was also determined for the t_0 coupons, which reflects the extent of corrosion that took place from the initial exposure to the bentonite, up to the point at which the cells were sealed. The mean loss of material that occurred on the t_0 specimens was subtracted from that measured on each of the tested coupons to allow determination of the extent of corrosion that took place once the cells were sealed (i.e., the test period) as shown in Figure 3-7. As corrosion was expected to halt on the development of anoxia in the glass cells, an oxidic corrosion rate could have been determined considering the duration of exposure from assembly until all the oxygen was consumed (as indicated by the oxygen spots). However, this approach was disregarded as oxygen might have been present in the bentonite after depletion of the head space. The presence of a copper and iron sulphide corrosion product in Cell S3 (Figure 3-12) also suggests that anoxic corrosion had occurred in the tipped cell.

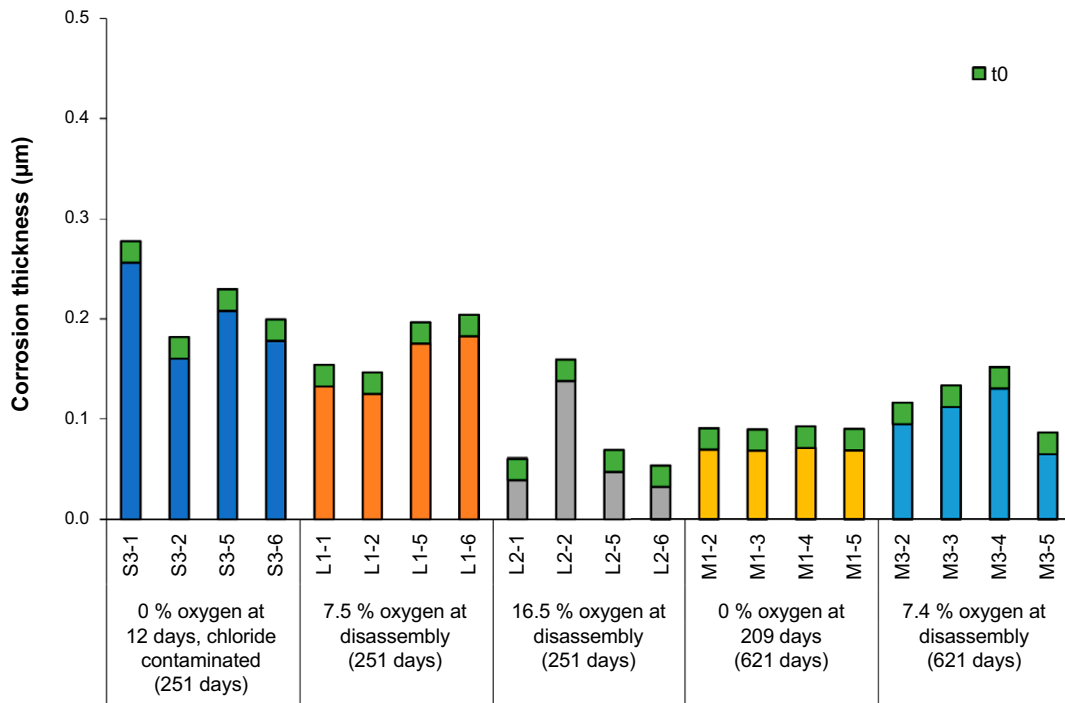


Figure 3-7. Total corrosion thicknesses for the copper coupons removed from the small cell (S3) and the large cells (L1 and L2) after 251 days, as well as the medium cells (M1 and M3) after 621 days. The amount of corrosion that is anticipated to have occurred prior to sealing the vessels (based on the t_0 coupons) is highlighted in green, with the remainder being the test corrosion thickness. Glass cells were operated at 50 °C. Moisture contents at disassembly: S3, 27.7 %; L1, 12.0 %; L2, 12.8 %; M1, 13.5 %; M3, 8.2 %.

Table 3-6 summarises the results of the corrosion rate measurements for the disassembled cells. From the corrosion loss, the corrosion rate was calculated, with CR_{total} reflecting the corrosion rate based on the total mass loss and CR_{test} reflecting the corrosion rate after subtraction of the mass loss observed in the t_0 tests. Figure 3-8 shows the calculated values of CR_{total} for specimens taken from each of the disassembled cells. The contribution of corrosion prior to sealing the vessels, as determined by the mass loss of the t_0 specimens, is highlighted in green (equivalent to $0.03 \mu\text{m yr}^{-1}$ for 251 day cells and $0.01 \mu\text{m yr}^{-1}$ for 614 day cells), with the CR_{test} values indicated by the lower portion of each bar.

Table 3-6. Corrosion rates for the copper coupons exposed in the glass cells for 249 days (S3, L1, L2) and 614 days (M1 and M3), including the thickness loss measured on the t_0 cells (the mean value was used to correct corrosion rates for the other cells, i.e. to convert 'total corrosion rate' into 'test corrosion rate'). Glass cells were operated at 50 °C.

Cell # (Cell Volume, %O ₂ at dismantling)	Coupon name	Total Thickness loss (μm)	Total corrosion rate ($\mu\text{m yr}^{-1}$)	Test corrosion rate ($\mu\text{m yr}^{-1}$)	Mean test corrosion rate ($\mu\text{m yr}^{-1}$) ⁶	Standard deviation of test corrosion rates ($\mu\text{m yr}^{-1}$)
S3 (0.20 L, 0 %) ⁷	S3-1	0.28	0.41	0.38	0.30	0.06
	S3-2	0.18	0.27	0.24		
	S3-5	0.23	0.34	0.31		
	S3-6	0.20	0.29	0.26		
L1 (0.75 L, 7.5 %)	L1-1	0.15	0.23	0.20	0.23	0.04
	L1-2	0.15	0.22	0.18		
	L1-5	0.20	0.29	0.26		
	L1-6	0.20	0.30	0.27		
L2 (0.75 L, 16.5 %)	L2-1	0.06	0.09	0.06	0.10	0.07
	L2-2	0.16	0.23	0.20		
	L2-5	0.07	0.10	0.07		
	L2-6	0.05	0.08	0.05		
M1 (0.40 L, 0 %)	M1-1	0.09	0.05	0.04	0.04	0.00
	M1-2	0.09	0.05	0.04		
	M1-5	0.09	0.05	0.04		
	M1-6	0.09	0.05	0.04		
M3 (0.40 L, 7.4 %)	M3-1	0.12	0.07	0.06	0.06	0.02
	M3-2	0.13	0.08	0.07		
	M3-5	0.15	0.09	0.08		
	M3-6	0.09	0.05	0.04		
t_0 (N/A)	t_0 -1	0.01	N/A	N/A	0.01/0.03 ⁸	< 0.01
	t_0 -2	0.03				
	t_0 -5	0.02				
	t_0 -6	0.02				

⁶ Calculated from the test corrosion rate.

⁷ Cell S3 was tipped at 4 days and was subsequently contaminated with a saturated sodium chloride solution.

⁸ This is the value subtracted from the total corrosion rate to give the test corrosion rate for the 614 and 249 day tests, respectively.

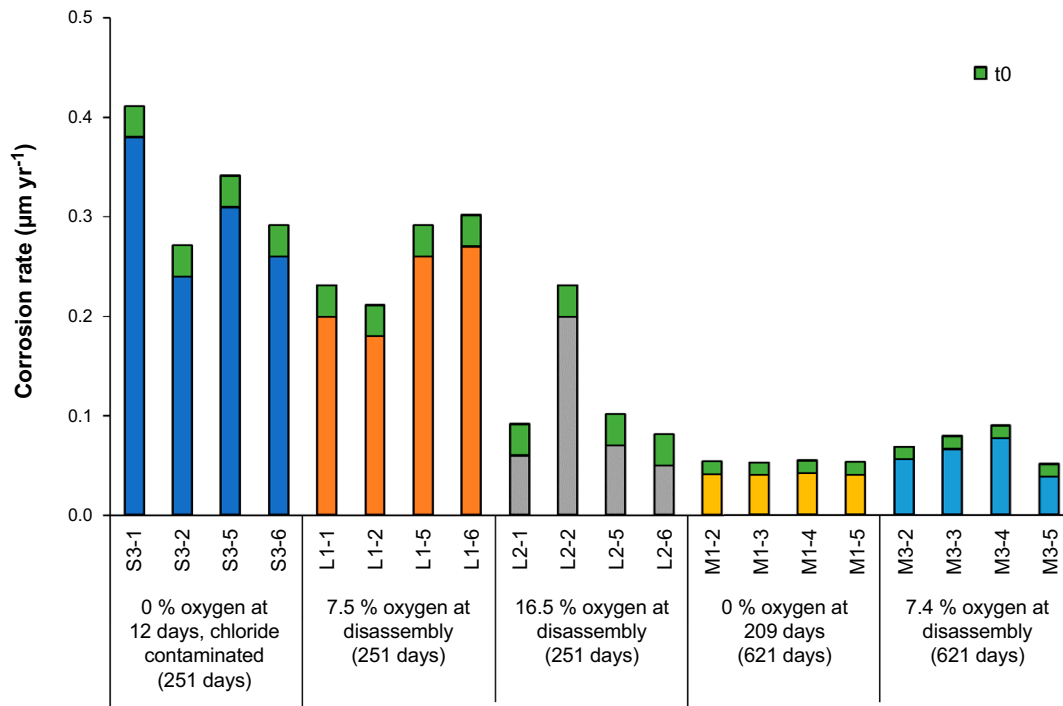


Figure 3-8. Average corrosion rates for the copper coupons removed from the small cell (S3, which was tipped over) and the large cells (L1 and L2) after 251 days, as well as the medium cells (M1 and M3) after 621 days. The amount of corrosion that is anticipated to have occurred prior to sealing the vessels (based on the t_0 coupons) is highlighted in green, with the remainder being the test corrosion rate. Note, that conversion of the t_0 mass loss is dependent on the duration of exposure, which was different for the large and medium cells. Glass cells were operated at 50 °C. Moisture contents at disassembly: S3, 27.7 %; L1, 12.0 %; L2, 12.8 %; M1, 13.5 %; M3, 8.2 %.

Unsurprisingly, the highest corrosion rates were observed in Cell S3 ($0.30 \mu\text{m yr}^{-1}$), which tipped over, exposing the coupons to saturated salt water. Comparing cells L1 and L2 shows that the coupons in Cell L1 exhibited a higher CR_{test} on average ($0.23 \mu\text{m yr}^{-1}$) when compared to Cell L2 ($0.10 \mu\text{m yr}^{-1}$), despite exhibiting a lower oxygen concentration throughout the test⁹. It should also be noted that the variation in corrosion rates observed between coupons in the same cell was rather high, as indicated by the standard deviations reported in Table 3-6 and the individual results shown in Figure 3-8. This can be accounted for by the uncertainty of the measurements which had a maximum of $\pm 0.123 \mu\text{m yr}^{-1}$ with a confidence of 95 %. This indicates that the difference in mass loss between individual coupons in the large cells, and between the cells themselves is not statistically significant.

Cells M1 and M3 were dismantled after 614 days to allow further assessment of the influence of oxygen depletion on the average corrosion rate. The oxygen concentration in Cell M1 decreased up to 209 days, at which point oxygen was fully depleted and the cell remained anoxic for the rest of the experiment. The oxygen concentration in Cell M3 decreased over the full exposure period of 614 days to a minimum value of 7.4 % (comparable to the final oxygen concentration in Cell L1). The average corrosion rate in Cell M1 was $0.04 \mu\text{m yr}^{-1}$ with excellent repeatability between the four individual coupons. The average corrosion in Cell M3 was higher than M1, with a mean of $0.06 \mu\text{m yr}^{-1}$ measured across the four coupons. The absolute difference between the average corrosion rates of the two cells is only $0.02 \mu\text{m yr}^{-1}$, which reflects a higher corrosion rate in M3 compared to M1 of 1.5 times as great. However, when the corrosion rates are considered alongside the measurement uncertainty for the medium cells ($0.046 \mu\text{m yr}^{-1}$, 95 % confidence) the difference between the cells was not significant.

⁹ If the corrosion rate of the copper was fast enough to significantly consume the oxygen in the cell over the test duration, then it would be expected that the cell with the lower oxygen concentration would have the most corroded coupons. However, the oxygen concentration in the cell is largely independent of the extent of copper corrosion and is instead dominated by stainless steel corrosion and possibly interaction with the bentonite.

Comparison of the average corrosion rate of Cell M3 ($0.06 \mu\text{m yr}^{-1}$) to Cell L1 ($0.23 \mu\text{m yr}^{-1}$) shows that the corrosion rate was much lower in M3, despite the cells exhibiting similar final and average oxygen concentrations (see Table 3-2). This suggests that the corrosion rate exhibits an attenuation in rate over time given that cell M3 was tested for 614 days as opposed to 249 days. This is consistent with the observations made from comparison of the L1 and L2 cells that suggest the corrosion rate in the large cells were not heavily influenced by oxygen concentration.

3.4.2 XPS

Table 3-7 presents the surface elemental concentrations obtained by XPS analysis for copper coupons L1-4, L2-4, and S3-4. Three points on each of the coupon surfaces were analysed, the last point (Point 3) was also analysed after ion bombardment. A selection of fitted XPS spectra are presented in Figure 3-9 to Figure 3-11. The full set of XPS spectra pre- and post-ion bombardment are available on request.

Table 3-7. XPS surface concentration (S) results for L1-4, L2-4 and S3-4 copper coupons. Surface concentrations post-depth profiling¹⁰ (DP) with Ar⁺ ion bombardment are also presented. Note that C (herein referred to as ‘adventitious’ carbon) is often found on XPS measurements before depth profiling.

S/DP	Element concentration (normalised at. %)									
	C	O	Cu	Cl	S	Si	Na	Mg	N	Ca
L1-4 (0.75 L, 7.5 % O₂, 249 days)										
S	44.2	41.1	11.1	0.4	Trace	3.2	-	-	-	-
DP	9.6	48.2	39.2	-	1.3	1.7	-	-	-	-
L2-4 (0.75 L, 16.5 % O₂, 249 days)										
S	46.7	29.1	12.1	1.3	-	4.1	0.9	-	5.7	-
DP	3.9	9.8	86.3	-	-	-	-	-	-	-
S3-4 (0.20 L, 0 % O₂, 249 days)										
S	20.6	47.9	6.6	2.3	3.4	14.8	2.0	1.4	-	0.9
DP	3.7	40.4	32.1	3.5	-	14.7	4.1	1.5	-	-

¹⁰ The depth of ablation achieved during depth profiling was not quantified but has been estimated in the range of several nm based on the ranges in rates of ablation of other materials.

L1-4 (0.75 L, 7.5 % O₂, 249 days)

A large amount of adventitious carbon was present on the as-examined coupon (44.2 at. %), along with oxygen (41.1 at. %) and copper (11.1 at. %). Following depth profiling the carbon concentration decreased to 9.6 at. %, and a larger proportion of oxygen (48.2 at. %) and copper (39.2 at. %) was observed. Small amounts of sulphur (1.3 at. %), and silicon (1.7 at. %) were also present post-depth profiling. High resolution spectra in Figure 3-9 show that, prior to depth profiling, the Cu2p and Cu L₃M_{4,5}M_{4,5} spectra were consistent with the presence of spertiniite (Cu(OH)₂) and a small amount of cuprite (Cu₂O). The proportion of cuprite compared to spertiniite increased after depth profiling. The S2p spectrum presented with two distinct peaks, one characteristic of sulphide and the other sulphate. Due to the trace concentration of sulphur on the surface one cannot reliably determine the exact binding energy of the components past them being characteristic of a sulphide and sulphate. The C1s spectra showed a peak characteristic of carbonate at 289.7 eV (spectra not included in below figure) and this peak remained post-depth profile, indicating it is present throughout the depth of profiled material.

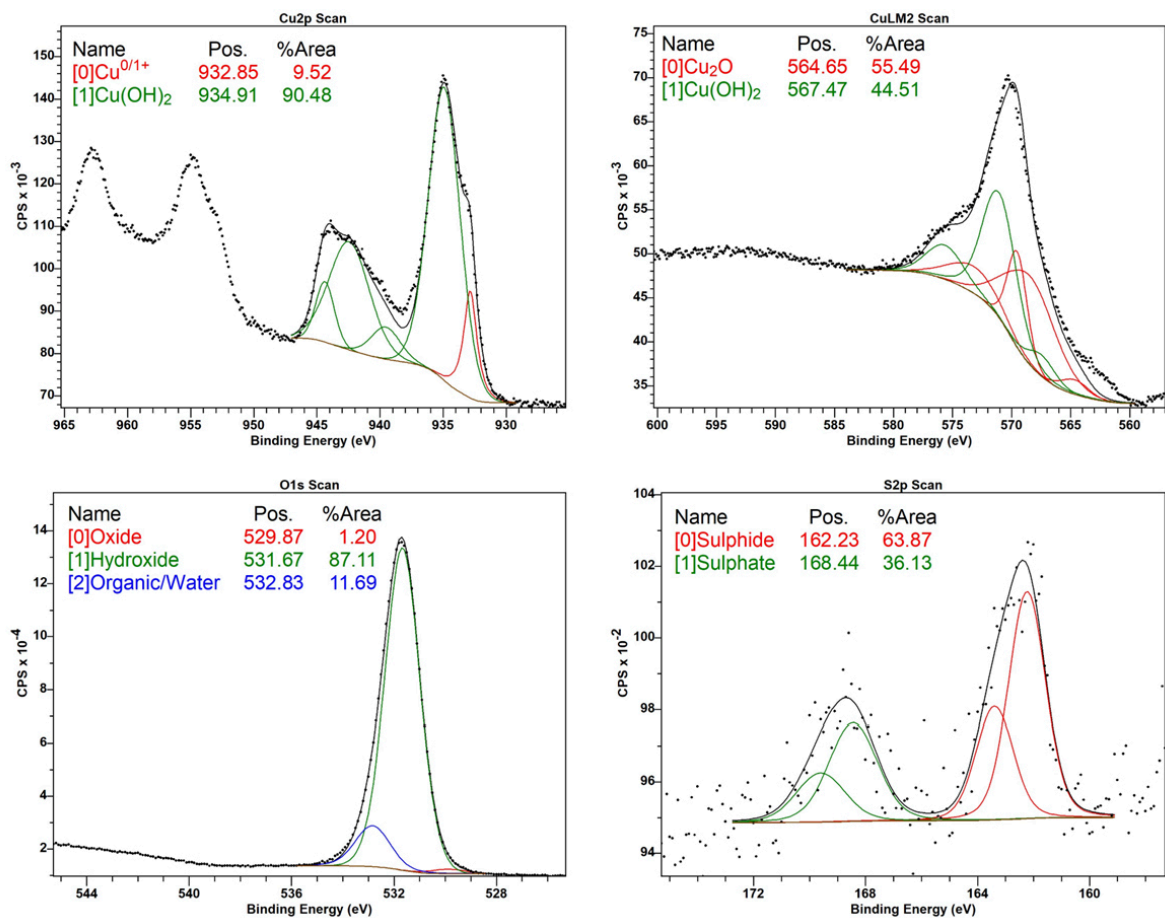


Figure 3-9. Representative XPS spectra of L1-4 (0.75 L, 7.5 % O₂, 249 days) surface profile.

L2-4 (0.75 L, 16.5 % O₂, 249 days)

As with copper coupon L1-4 previously discussed, L2-4 had a large amount of adventitious carbon on its surface (46.7 %). Oxygen (29.1 %) and copper (12.1 %) were also present surface profiling, along with smaller amounts of silicon (4.1 %), chlorine (1.3 %), and sodium (0.9 %). It is possible that these trace elements are associated with residual adherent bentonite on the specimen surface. High resolution Cu2p and Cu L₃M_{4,5}M_{4,5} spectra were largely consistent with the presence of spertiniite and cuprite (see Figure 3-10). The Cu2p spectrum showed that cuprite was the main copper species on the surface of L2-4, contrasting to L1-4 where spertiniite was the dominant species in the Cu2p spectrum surface profile. Minimal carbonate was observed on L2-4, unlike L1-4 where a clear component was identified in the C1s spectrum. Following depth profiling a small amount of carbon was present (3.9 %), with the rest of the area comprising oxygen (9.8 %) and copper (86.3 %). Cuprite was shown to increase in relation to spertiniite post-depth profile, as seen on L1-4.

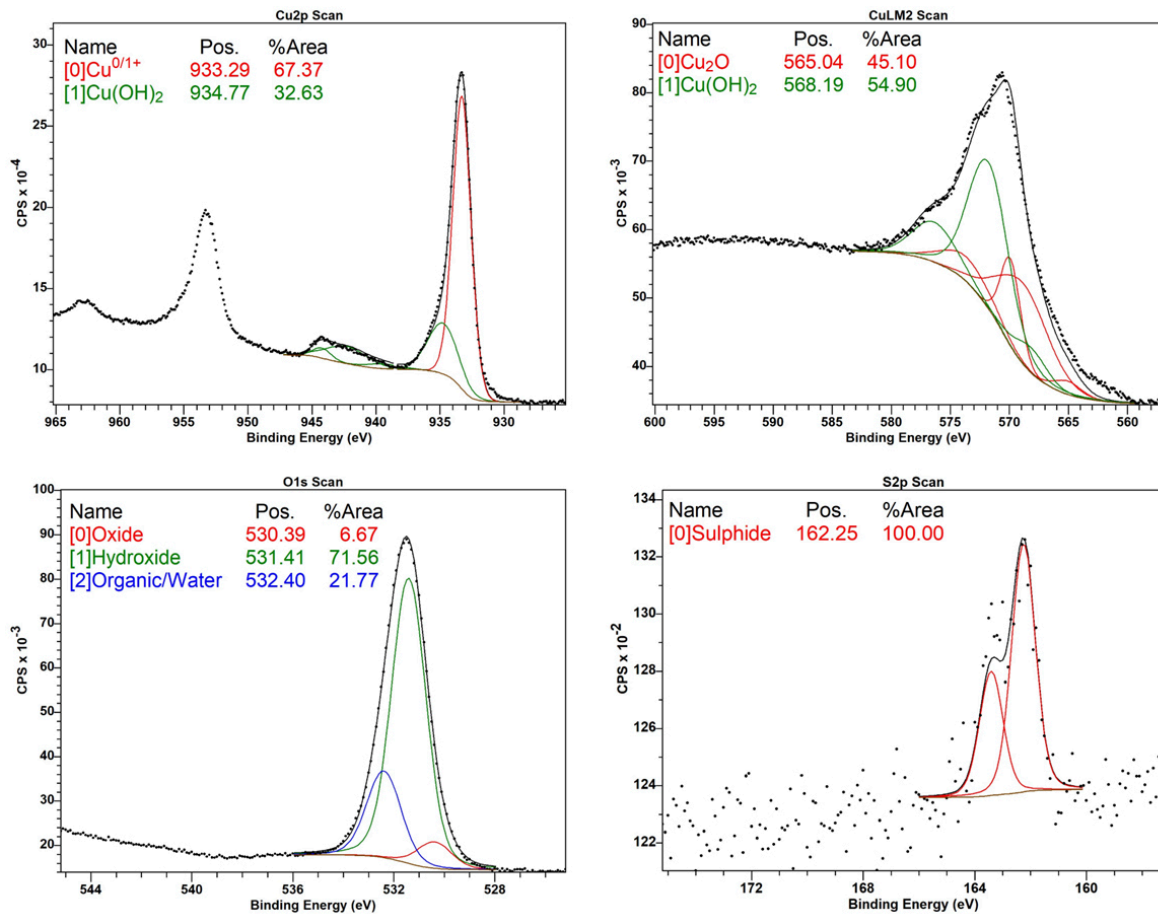


Figure 3-10. Representative XPS spectra of L2-4 (0.75 L, 16.5 % O₂, 249 days) surface profile.

S3-4 (0.20 L, 0 % O₂, 249 days, chloride contaminated)

Pre depth-profile, the elemental composition consisted of carbon (20.6 %), oxygen (47.9 %), and silicon (14.8 %), with a smaller proportion of copper (6.6 %). The Cu2p and Cu L₃M_{4,5}M_{4,5} spectra shown in Figure 3-11 were consistent with a mixture of chalcocite (Cu₂S) and cuprite. The S2p spectrum was also characteristic of a sulphide, which is in agreement with the assignment of chalcocite in the copper spectra. After depth profiling the silicon content was largely the same (14.7 %), with greater contributions from oxygen (40.4 %) and copper (32.1 %) following the removal of adventitious carbon. The presence of a high proportion of silicon is indicative of the presence of adherent bentonite.

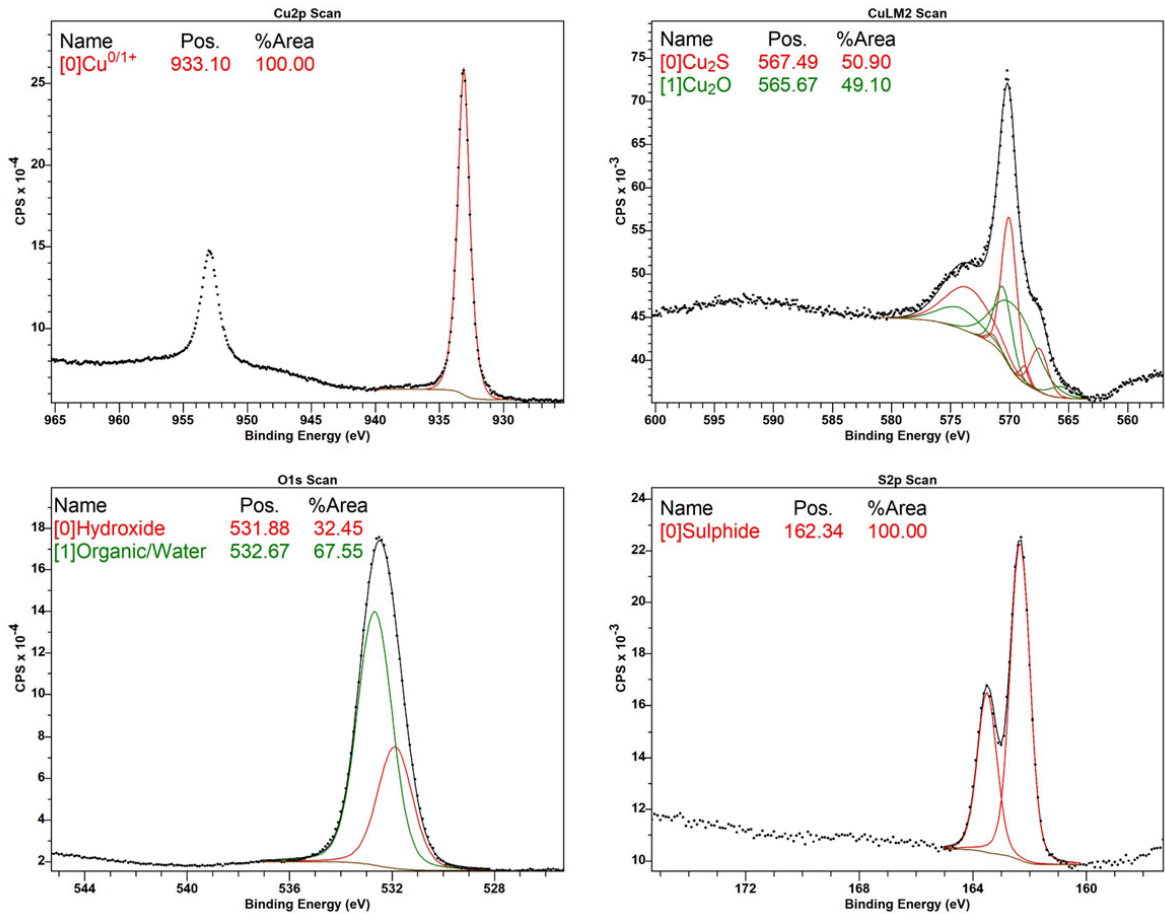


Figure 3-11. Representative XPS spectra of S3-4 (0.75 L, 0 %) surface profile.

3.4.3 Raman spectroscopy

Raman spectroscopy was carried out on 3 coupons in total. One coupon was analysed from each of the glass cells dismantled after 249 days (S3, L1 and L2). Identification of corrosion products and bentonite was carried out by comparison to specimens in the RRUFF database¹¹. Compounds were chosen from the database based on their chemical formula. The limitations of this method for identification are that the specimens in the database are well characterised and homogenous, compared to the heterogeneous products associated with the coupon surfaces. The consequence of this is that additional unidentifiable peaks might be observed in the spectrum, or peaks may have shifted due to the presence of impurities in the products or subtle differences in the chemical structure (non-stoichiometric copper oxides etc.). With these limitations in mind, the identification of compounds in Table 3-9 is accompanied with a confidence score according to the qualification set out in Table 3-8. The identification procedure considered peaks up to a wavenumber shift of 1 000 cm⁻¹.

Table 3-8. Qualifying criteria for the assignment of compound identities using Raman spectroscopy.

Confidence	Qualification
Low	Some main peaks identified, but the ratio of them is not consistent with the compound in the database. Some main peaks identified, but the spectrum is not wholly consistent with the compound.
Medium	Most of the main peaks identified, limited ambiguity in terms of peaks aligning with alternative compounds.
High	Strong fit with the compound in the database.

The Raman spectra for coupons L1-3 and L2-3 showed similar spectra to each other, consistent with the presence of cuprite (Cu₂O). An additional peak at 520 cm⁻¹ tentatively indicated the presence of spertiniite (CuOH₂) on both coupons as well. The peaks on L2-3 were stronger and the broad fluorescence associated with montmorillonite (associated with the bentonite) was also weaker when compared to L1-3. The spectra for S3-3 showed a broad peak at 310 cm⁻¹, which is consistent with the spectra of bornite (Cu₅FeS₄). Tenorite (CuO) also shows a peak at 310 cm⁻¹, but the peak is typically sharp compared to the broader peak associated with bornite. Broad fluorescence associated with montmorillonite (associated with the bentonite) was also observed on the spectra of S3-3. Note that the broad fluorescence from the montmorillonite has been subtracted from the spectra.

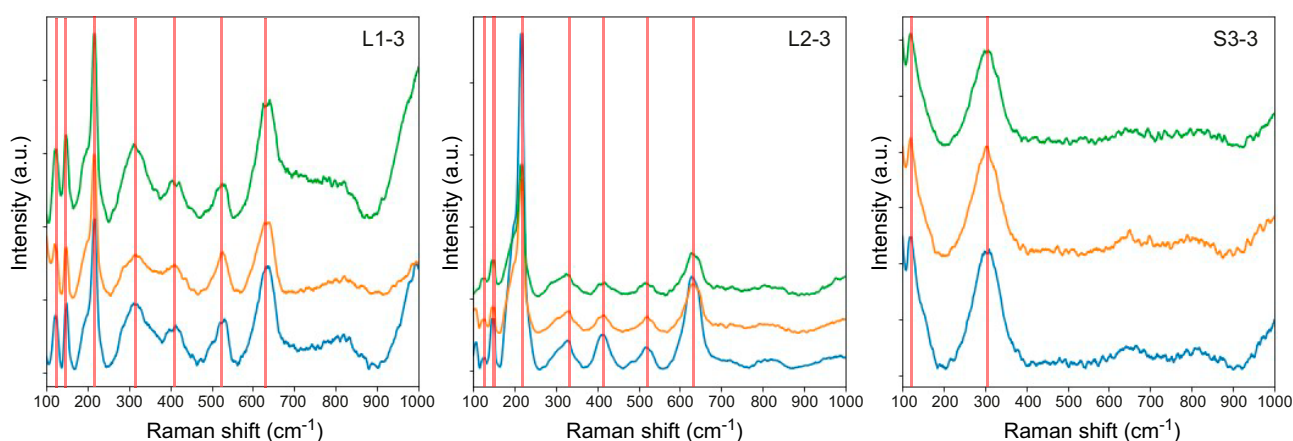


Figure 3-12. Representative Raman spectra obtained from copper coupons L1-3 (0.75 L, 7.5 % O₂, 249 days), L2-3 (0.75 L, 16.5 % O₂, 249 days), and S3-3 (0.20 L, 0 % O₂, 249 days, NaCl contaminated). Broad fluorescence associated with montmorillonite has been subtracted from the spectra.

¹¹ <https://rruff.info/>

Table 3-9. Identification of Raman active compounds on copper coupons L1-3 (0.75 L, 7.5 % O₂), L2-3 (0.75 L, 16.5 % O₂) and S3-3 (0.2 L, 0 % O₂, NaCl contaminated). Confidence in identification assigned according to Table 3-8.

Peak cm ⁻¹	Coupon numbers	ID	Confidence
120	L1-3 L2-3 S3-3	Cuprite Cuprite N/A	H H
150	L1-3 L2-3	Cuprite Cuprite	H H
220	L1-3 L2-3	Cuprite Cuprite	H H
310	S3-3	Bornite Tenorite	M L
330	L1-3 L2-3	Cuprite Cuprite	H H
420	L1-3 L2-3	Cuprite Cuprite	H H
520	L1-3 L2-3	Spertiniite Spertiniite	L L
640	L1-3 L2-3	Cuprite Cuprite	H H
Broad rise (subtracted from spectra)	L1-3 L2-3 S3-3	Montmorillonite Montmorillonite Montmorillonite	H H H

4 Discussion

4.1 Comments on test methodology validation

Initial testing of the oxygen sensor spots successfully validated several assumptions associated with the test configuration. The oxygen sensor spots provided an effective solution to monitoring the oxygen concentration within the headspace of sealed glass cells. Owing to the non-destructive properties of the sensing technique, changes to oxygen concentration over time within the range of interest was achieved without disturbing the internal conditions. The oxygen sensor spots also allowed the consumption of oxygen within the glass cells to be compared, with smaller cells depleting faster than larger cells. Corrosion rates of the copper coupons were determined using mass loss since the rate of oxygen consumption could not be used to calculate the copper corrosion rate, as discussed in Section 4.2. The corrosion products that formed on the coupons were characterised using Raman spectroscopy and XPS, indicating that the dominant species present was cuprite, which was identified at two different final oxygen concentrations (7.5 and 16.5 %).

During the test programme, several issues were identified that placed limitations on the usability of the results. Mitigations for these issues are discussed in Section 4.4. The geometry of the small and medium glass cells made them prone to tipping. A few of the glass cells tipped upon initial placement in the 50 °C oven, along with an additional glass cell being tipped because of human error. Disturbance of the glass cells in the oven was mitigated using a walled tray, but the removal of human error could not be achieved as oxygen measurements required physical manipulation of the cells. None of the large cells were tipped during the experiment due to their wider base. Once tipped, the stainless steel sample holders containing the bentonite were contaminated with the saturated sodium chloride solution originally contained in the glass cell reservoirs (Figure 2-2). The oxygen in the tipped cells was consumed in days, decreasing the amount of repeat tests available for analysis (Figure 3-1, Figure 3-2 and Figure 3-4). Dismantling of a tipped cell (S3) revealed significant corrosion of the stainless steel sintered filter (Figure 4-1), partial saturation of the contained bentonite (Table 3-5), deposition of red corrosion products (presumably iron oxides) in the bentonite (Figure 4-1), and potentially the formation of bornite (Cu_5FeS_4) (Table 3-9). The above observations indicate that the stainless steel was probably responsible for the oxygen consumption rather than the copper coupons in the tipped cells. While the stainless steel might not be expected to corrode in conditions of limited corrosivity, the saturated chloride solution provided a harsh environment, and the porosity (33 to 38 %) of the stainless steel filter provided a large surface area for corrosion to take place. As a result of the tipping event and the contact with salt water, the bentonite moisture content of cell S3 was 27.7 wt. %.



Figure 4-1. Images of the stainless steel sample holder (upper left) and steel filter (lower left) and the bentonite (right) from tipped glass cell S3 (0.20 L, 0 % O_2 , 249 days, NaCl contaminated).

Experimentally derived water retention curves for MX-80 bentonite in a 50 °C and 75 % RH environment suggest the bentonite should have a moisture content of ~ 14.0 wt. % (Dueck and Nilsson 2010). Therefore, the tipping of cell S3 significantly increased the bentonite moisture content. Three of the cells examined (L1, L2 and M1) had moisture contents comparable to the water retention curves (~ 12.8 wt. %). However, cell M3 had a lower moisture content of 8.2 wt. %. Some reduction of the moisture content in the bentonite after exposure is expected due to being dismantled in the glove box environment (24 °C, ~0 % RH), but it is unclear why cell M3 exhibited lower moisture contents than the other cells that were not tipped.

The starting oxygen concentration in individual glass cells exhibited a modest variability, probably because of a small amount of oxygen being consumed in the glass blowing process used to seal the glass cells. Additionally, there was a significant difference in the rate of oxygen consumption in glass cells that were nominally identical. In some circumstances the rate of oxygen consumption seemed to change within specific cells but not others. This observation was particularly apparent in glass cell L1, in which the oxygen consumption rate accelerated after 174 days (Figure 3-3), this was not observed in other cells.

Perhaps more importantly, white crystals were observed on most of the stainless steel sample holders, and the base of the sample holders showed visible signs of localised corrosion (Figure 4-2). The white crystals might have been sodium chloride; however, the deposition also occurred in glass cells that had not been tipped suggesting that unexpected chemical processes might have been occurring in the cells. Beyond the localised corrosion of the base of the sample holders, no further visible corrosion of the stainless steel including the filters was observed in the non-tipped cells. Follow up analysis revealed that the pH of the reservoir water in glass cell L1 was approximately 2.8 (Table 3-4), and IC analysis (not shown) of the water revealed the presence of an organic acid (probably acetic acid). Inspection of the technical specification of the silicone rubber compound (RS Components Ltd 2023) used to line the reservoirs (to prevent salt creep) revealed it contained methyltriacetoxysilane, which liberates acetic acid on contact with moisture (<https://pubchem.ncbi.nlm.nih.gov/compound/77929#section=Names-and-Identifiers>). Acetic acid is highly volatile and probably caused corrosion of the stainless steel which in turn consumed the oxygen in the headspace. This hypothesis was further backed up by the high rate of oxygen consumption which was far greater than what could be achieved from the corrosion of the copper coupons alone (Section 3.2) and by the fact that the rate of oxygen consumption in the cell containing stainless steel alone was similar to that of experimental cells.



Figure 4-2. Images of the white crystals formed on M1 (left), and of the corrosion of the stainless steel sample holder bases of L1 (middle) and L2 (right).

4.2 Influence of oxygen on corrosion rate

As discussed above, during testing some of the glass cells were inadvertently tipped over. When this occurred, this was followed by an increased rate of oxygen consumption leading to depletion of the oxygen in the cell within a few days. These and other results (Section 4.1) strongly indicate that, in these cells, the cause of the rapid depletion in oxygen was the corrosion of the stainless steel filters by the saturated sodium chloride solution that came into contact with it upon tipping.

In glass cells that were not tipped over, there was still a high variability in the rate of oxygen consumption. The results described in (Section 4.1) indicate this to be caused by leaching of acetic acid from the silicone rubber compound that was used to prevent salt creep corroding the external surface of the stainless steel even in the absence of bulk water phases in contact with it (Section 4.1). No evidence of acetate species was observed on the copper coupons, and the pH of the bentonite remained alkaline (Table 3-4). Based on these observations and the very low corrosion rates of the copper it is unlikely that the acetic acid penetrated the bentonite.

In all cells, the oxygen consumption rate was much higher than is predicted by copper corrosion alone (Figure 3-6), indicating that copper corrosion had little bearing on the concentration of oxygen within the cells. This is supported by the measurements obtained from the stainless steel only control cell, which exhibited a similar rate of oxygen consumption to the other cells (Figure 3-5). It should also be noted that in the stainless steel only control cell there was no bentonite, so oxygen consumption was constrained to that of the sample holder only.

Due to the reasons described above, it was not possible to determine changes in copper corrosion rate over time from the rate of consumption of oxygen in the test cells. Instead, the average corrosion rate was determined after different durations based on the mass loss of the corrosion coupons. The average copper corrosion rates were comparable to those expected for copper under extremely mild atmospheric exposure (level C1/ lower end of C2¹² in BS EN ISO 9224:2012 (BS EN ISO 2012)) and are lower than those exposed to bentonite saturated by oxalic Äspö groundwater over a comparable exposure period (Rosborg et al. 2011). The lower than anticipated corrosion rate could be caused by two mechanisms: (i) A lack of water in the bentonite (~8–13 wt.%), causing the corrosion rate to be limited by surface wetting rather than oxygen transport. This would cause the corrosion rate to be largely independent of the bulk oxygen concentration in the range (7.4 to 19.2 %) investigated. (ii) Poor availability of oxygen in the bentonite, which could mean the bulk oxygen concentration in the headspace of the glass cell had little bearing on the conditions seen by the coupons in the bentonite. The observation that the bentonite was relatively dry (Table 3-5) and uncompacted at the end of the test implies that oxygen transport through it would be reasonably unhindered. However, given that bentonite can consume oxygen (Åkesson and Laitinen 2022) and oxygen might adsorb to bentonite (Burzan et al. 2022), it may be possible for an oxygen gradient to exist within it despite the presence of the pore spacing. In both instances, it would be expected that if the oxygen concentration dropped further there would be an attenuation in corrosion rate below some critical concentration.

The average corrosion rates of the copper coupons in L1 ($0.23 \mu\text{m yr}^{-1}$) were higher than L2 ($0.10 \mu\text{m yr}^{-1}$) despite the lower average oxygen concentration measured in L1. This observation would seem to be logical if the copper was consuming the oxygen, however due to the low corrosion rate of the copper and the consumption of oxygen by other processes (stainless steel corrosion and bentonite reactions) the results are inconsistent with the expected mechanism of lower oxygen leading to a reduced corrosion rate. It is therefore not clear why a higher corrosion rate was observed in conditions where the oxygen concentration was lower. The measurement uncertainty of the mass loss in the large cells indicated that the results were not significant. As such the variance in corrosion rates among specimens within the same test suggests that factors other than oxygen levels influenced the rate. This is consistent with the view that surface wetting (related to RH) had a more dominant role than oxygen availability in these tests. Note that this observation is based on the mass loss of eight coupons in two cells. The influence of uncertainty on the findings could be reduced by measuring more coupons, as well as by prolonging the experimental duration.

¹² Upper limit for C1 is $0.1 \mu\text{m yr}^{-1}$, upper limit for C2 is $0.6 \mu\text{m yr}^{-1}$ for the first year of exposure.

Further elucidation of the influence of oxygen concentration on the corrosion of the copper was attempted by analysing two medium cells dismantled after 614 days: M1 that was anoxic after 209 days, and M3 that had a final oxygen concentration of 7.4 %. Both cells exhibited low corrosion rates overall, which increases the risk that any differences observed may be attributable to random variation. If the corrosion rate remained constant over time and stopped entirely once the cell was depleted of oxygen, then it would be expected that M1 would exhibit a corrosion rate of roughly one third of that observed in M3, which would correspond to an average corrosion rate of $0.2 \mu\text{m yr}^{-1}$. The corrosion rate that was observed was $0.4 \mu\text{m yr}^{-1}$, equivalent to roughly two thirds of that observed in M3. This could be explained by an attenuation in corrosion rate over time, which would mean most of the mass loss due to corrosion occurs during the initial period of the test. Hence, the average corrosion rate is disproportionately influenced by the corrosion behaviour at shorter durations. As with the large cells, the uncertainty associated with the mass loss measurements indicates that the difference between the two cells is not significant. Therefore, while these results are consistent with a decrease in corrosion rate following the consumption of oxygen they are not conclusive and could be attributable to random variation.

Overall, modification of the tests is required to improve the confidence in the corrosion rates, and to also identify the key parameters controlling copper corrosion in an oxic environment. Suggested modifications are discussed in Section 4.4.

4.3 Nature of corrosion product

Based on analysis of coupons taken from the large cells, there was no impact of the different oxygen concentrations on the corrosion products produced during the test. This supports the conclusions drawn from the mass loss results, namely that the difference in the average corrosion rates of coupons from the glass cells L1 and L2 was not attributable to differences in oxygen concentration. Raman spectroscopy and XPS analysis of the corrosion products on the copper coupons from the two large cells were consistent with the presence of cuprite (Cu_2O) and spertiniite ($\text{Cu}(\text{OH})_2$). Small amounts of sulphides were also identified by XPS analysis, however they were not consistent with copper sulphides (Figure 3-9 and Figure 3-10). The presence of silicon on the coupons (Table 3-7) suggests the sulphides are probably attributed to adhered bentonite. The proportions of cuprite and spertiniite identified by XPS were roughly equal, while the Raman spectra were more consistent with cuprite, with limited evidence for spertiniite. The discrepancy between the Raman spectroscopy and XPS results probably arises from the differences in surface sensitivity between the two techniques. The typical analysis depth of Raman spectroscopy is approximately $3 \mu\text{m}$, which is more representative of the bulk corrosion product, compared to the 10 nm analysis depth of XPS. The predominance of the Cu(I) oxide cuprite on the coupons suggests that full oxidation of the copper metal to Cu(II) (in this case spertiniite) was restricted despite the high concentration of oxygen in the glass cell headspace and may thus indicate that oxygen availability in the bentonite was relatively poor.

In the tipped glass cell (S3) the XPS spectrum was consistent with approximately equal amounts of copper sulphide and cuprite. A small amount of sulphur (identity not determined) was also present post depth-profiling. Similarly, the Raman spectroscopy suggested the presence of the copper and iron-containing sulphide bornite (Cu_3FeS_4), although it is possible that tenorite was also present, but the Raman spectrum was inconclusive. The corrosion products present on the copper coupon from the tipped small cell suggest both oxic and anoxic corrosion occurred. The oxic corrosion was probably responsible for the formation of cuprite, and the anoxic corrosion for the formation of bornite. The presence of sulphide containing corrosion products (see Sections 3.4.2 and 3.4.3) can indicate the possibility of microbially influenced corrosion arising due to the action of sulphate reducing bacteria (SRB) within the bentonite. However, in the present work this is unlikely due to the combination of two factors. 1. SRB are anaerobic (Pereira et al. 2011), so it is expected that sulphide reduction could only occur following consumption of oxygen in the cells, i.e., after 12 days. 2. After the cell had been contaminated with the saturated salt solution a high salinity/low water activity environment would have been established in the experiment inhibiting microbial activity (Brown 1976). Bornite is not typically identified on corroded copper from in situ experiments (Wersin 2013, Gordon et al. 2017, 2018, Johansson et al. 2020). However, the conditions the copper was exposed to in the tipped glass cell were not typical of an in situ environment. The contact of the saturated sodium chloride

solution with the high porosity stainless steel filter left an abundance of iron corrosion products in the bentonite. The pH of the bentonite porewater may have also been different to the non-tipped cells but was not measured (Table 3-4). Bornite has previously been observed in lab-scale studies on copper cylinders, capped with steel sintered filters and packed with bentonite (Vikman et al. 2018). In that instance the cylinders were exposed to oxic solution but were sealed for 15 years before examination, possibly allowing time for oxygen consumption to occur. Additionally, bornite has also been identified on the brass fittings of an iron plate helmet extracted from a clay soil during an archaeological excavation (Smart and Adams 2006).

4.4 Future work

While the in situ oxygen monitoring method and analysis of the corrosion rates and corrosion products was achieved with the techniques used in this study, a number of issues with the experimental method were identified (Section 4.1). Although not originally envisioned when the experiment was designed, it became apparent that the oxygen sensors could potentially be used to measure the corrosion rate of the copper coupons in situ in oxic conditions. However, the consumption of oxygen by the corroding stainless steel sample holders prevented the in situ copper corrosion rate measurements. Additionally, the stainless steel corrosion prevented the quantification of oxygen consumption by the bentonite. The stainless steel probably corroded due to the leaching of highly volatile acetic acid from the silicone rubber sealant that was used to prevent salt creep. In future the sealant could be cured beforehand to remove the acetic acid, or alternatively a pH neutral sealant (as opposed to an acid-based one) could be used. The corrosion of the stainless steel raised the concern around the use of potentially corrodible material in an experiment where the aim is to measure oxygen consumption by the corrosion of copper. Swelling of the bentonite is not a concern as it is pre-equilibrated to the RH of the experiment. Therefore, the glass cells could be assembled with no metallic components, with the bentonite and copper specimens contained within an internal glass/PTFE beaker. An additional benefit of the beaker configuration is that oxygen diffusion from the headspace of the ampoule to the coupons would happen only in one direction. As oxygen diffusion would be occurring in one direction it would be preferable to use holders that only expose one face of the coupons. The advantage of this setup is it is more amenable to modelling with a simple 1D model, which could be implemented alongside the experimental work to aid with interpretation of the results. This setup could also be used to investigate the consumption of copper and bentonite independent of other corrodents (i.e. stainless steel) so that individual oxygen consumption mechanisms can be accounted for. Different thicknesses of bentonite with and without copper specimens could also be employed to explore the impact the diffusion rate of oxygen through the bentonite has on the corrosion rate.

In situ measuring of the copper corrosion rate would also require optimisation of the experimental configuration. The headspace volume and the surface area of copper would need to be adjusted so the observed corrosion rates of roughly 0.1 to 0.2 $\mu\text{m yr}^{-1}$ deplete the oxygen over a short enough time scale to study (~6 months to a year). With the above parameters defined, the rate of oxygen consumption in each cell can be converted to an equivalent corrosion rate based on whether the formation of Cu(I) or Cu(II) corrosion products prevail (i.e., mass balance approach). The in situ measured corrosion rate can then be checked at the end of the test by measuring the corrosion rate gravimetrically. Increasing the number of coupons contained in each test would also increase the confidence in the corrosion rates observed by improving the ability to perform statistical analysis. Furthermore, a range of RH and temperature values could be tested to measure their influence on corrosion rates. Along with comparisons between oxygen consumption and mass loss, electrochemical and electrical resistance techniques could complement the measurement of in situ corrosion rates. Furthermore, electrochemical measurements could be used to measure the kinetics of the cathodic reaction as a function of oxygen concentration to better characterise the conditions under which corrosion is feasible.

As shown with the tipped cells the method of controlling the humidity using saturated salt solutions introduces the risk of contaminating the bentonite with hyper-saline solutions, which leads to increased corrosion of the copper coupons. The pre-humidification of the bentonite is necessary to prevent the swelling of the bentonite in the test vessel, but also to ensure the experiment is being conducted

at the correct RH. The risk of tipping can be prevented by using glass cells with wider bases. This was evidenced by the large cells where no tipping events occurred. A level of risk remains from the necessity of handling the glass cells to complete the oxygen spot measurements. However, this could be minimised by utilising holders to keep the glass cells steady during measurements.

Finally, the sealing of the glass cells using glass blowing techniques results in the consumption of a small amount of oxygen in a non-systematic way, causing some (modest) discrepancies in the starting oxygen concentration of individual glass cells. The discrepancies in starting oxygen concentration can be prevented by sealing the lids in place with epoxy resin as opposed to glass blowing. The sealing of glass cell joints using epoxy resin has been used in previous experiments by Amentum and has retained air tightness in sealed cells for over ten years.

5 Conclusions

Glass cells of different volumes ('small', 'medium' and 'large') were designed and trialled to track the consumption of oxygen by the corrosion of copper coupons in a partially saturated bentonite buffer. OFP copper coupons were embedded in bentonite with a dry density of 1.45 Mg m^{-3} inside a stainless steel filter and sample holder. The glass cells were maintained in a $50 \text{ }^\circ\text{C}$ oven for a minimum of 249 days. The novel use of optical oxygen sensor spots enabled the in situ monitoring of the oxygen concentration without having to terminate the experiments. The glass cells were removed from the oven for a short duration (~ 5 minutes) on a weekly basis to complete the oxygen concentration measurements. Three glass cells were sacrificed after 251 days so that the coupons could be analysed using mass loss, XPS and Raman spectroscopy. A further two glass cells were dismantled after 621 days to complete mass loss on the coupons. The key findings of the analysis were as follows:

- Oxygen was consumed in the test cells at different rates over the test duration. Contrary to initial expectations, the major cause of oxygen consumption was via corrosion of the base of the stainless steel sample holders, which was generated, or at least exacerbated, by the leaching of acetic acid from a silicone rubber compound used in the cells. In addition to that, during the course of the experiment, several test cells were accidentally tipped over, leading to corrosion of the internal stainless steel filters, which resulted in rapid depletion of oxygen in the cells. For cells that tipped over, contamination by salt water influenced the test environment for the copper coupons and meant that the test was no longer valid.
- Two large cells were sacrificed after 251 days, at which point their oxygen concentrations had reduced to 7.5 % and 16.5 %. A higher average corrosion rate, of $0.23 \text{ } \mu\text{m yr}^{-1}$ compared to $0.10 \text{ } \mu\text{m yr}^{-1}$, was observed in the cell that exhibited the lower oxygen concentration. The difference between these corrosion rates was not significant when the measurement uncertainty was considered. These results show that above a final oxygen concentration of 7.5 % a reduction in oxygen concentration in the headspace due to consumption by corrosion of the stainless steel sample holder did not lead to a reduction in the corrosion rate of the copper coupons in these cells.
- Two medium cells were sacrificed after 621 days, at which point their oxygen concentrations were 7.4 % and 0 %, with the 0 % cell having turned anoxic after 209 days of exposure. The cell that had turned anoxic exhibited a lower average corrosion rate than the cell containing residual oxygen ($0.04 \text{ } \mu\text{m yr}^{-1}$ compared to $0.06 \text{ } \mu\text{m yr}^{-1}$), which is consistent with a reduction in the corrosion rate of the copper coupons upon complete consumption of the oxygen within the cell by corrosion of the stainless steel sample holder. However, as above when measurement uncertainty is considered the results are not statistically significant. Therefore, the results could partly be attributed to random variation. The analysis considered eight corrosion coupons, and the significance of the finding could be improved by analysing more repeats.
- The corrosion products that formed on the copper coupons in the intact cells were consistent with the presence of the Cu(I) oxide cuprite (Cu_2O), and a minor amount of the Cu(II) hydroxide spertiniite ($\text{Cu}(\text{OH})_2$). The predominance of Cu(I) oxides indicates the full oxidation of the copper to Cu(II) was constrained during the experiment. This could suggest that the availability of oxygen at the coupon surfaces was limited by the presence of bentonite surrounding them. No copper sulphides were detected on any of the intact cell coupons analysed, but trace amounts of sulphide were associated with adhered bentonite. Copper sulphides were identified in the tipped cell and were tentatively attributed to the copper iron sulphide mineral bornite.
- In general, average corrosion rates for copper coupons were lower than anticipated across the set of experiments and were comparable to those expected during atmospheric corrosion in mild conditions. This may be attributable to the low moisture content in the bentonite, of 8.2–13.5 % because of the selected RH of 75 %. The bentonite remained “dry” and powdery.

Overall, the trial indicated several unexpected occurrences may warrant further investigation. These occurrences, along with recommended mitigation steps, are described below:

- In the current setup, the ability to measure the in situ corrosion rate of the copper coupons in bentonite in oxic, humid conditions as a function of the concentration of oxygen was prevented by the corrosion of the stainless steel components. Corrosion of the stainless steel was accelerated by the leaching of acetic acid from a silicone rubber compound used in the experimental configuration. Acetic acid leaching could be minimised by pre-curing the rubber compound or using a different compound all together. However, the presence of the stainless steel in its current geometry (filter) may still lead to some consumption of oxygen, owing to its comparatively high surface area. We therefore recommend adopting a configuration where the bentonite and copper coupons are housed in an open topped glass/PTFE holder i.e., all metal other than the corrosion test specimens is eliminated completely.
- As discussed above, the observed corrosion rates/products suggest that the availability of oxygen at the coupon interface may be reduced by the presence of the bentonite. Further work is required to understand the consumption of oxygen by copper and bentonite independent of each other. Additionally, a beaker-like vessel could be used to limit the diffusion of oxygen to a single direction. By evaluating different bentonite thicknesses, it could be possible to determine the extent to which bentonite limits the availability of oxygen at the coupon interface.
- The volume of oxygen in the current configuration is too large to be consumed by the corrosion of the copper over a suitable period (6 months to a year). For future testing, optimisation of the ratio of the headspace volume to the surface area of the copper could be achieved based on the results from the present study to ensure that oxygen consumption via corrosion occurs over the desired timeframe. This would then enable the oxic corrosion rate to be determined in-situ via the rate of depletion of oxygen, if validated with periodic mass loss measurements.
- The use of saturated salt solutions to maintain the humidity in the experimental cells introduces the risk of contaminating the bentonite and copper with hyper-saline solutions. Such contamination events make the experimental results unusable. This risk could be mitigated by using cells with a wider base that are less susceptible to tipping, as well as using cell holders to complete oxygen sensor measurements.
- Sealing the glass cells using glass blowing reduces the oxygen content inside the cell due to combustion and leads to a reduction in the initial oxygen concentration as well as discrepancies in the starting oxygen concentration between individual cells. We recommend sealing the glass using an epoxy resin in future testing to ensure the starting oxygen concentration is equal to the atmospheric partial pressure of O₂.

References

SKB's (Svensk Kärnbränslehantering AB) publications can be found at www.skb.com/publications. SKBdoc documents will be submitted upon request to document@skb.se.

Aggarwal S, Addepalli V, Smart N R, 2015. Further metallographic analysis of MiniCan SCC test specimens. SKB R-15-11, Svensk Kärnbränslehantering AB.

Andersson-Östling H C M, Hagström J, Danielsson M, 2018. Phosphorus in copper intended for spent nuclear fuel disposal. SKB R-17-19, Svensk Kärnbränslehantering AB.

ASTM, 2017. Standard Practice for Preparing, cleaning, and evaluating corrosion test specimens, ASTM G1-03 2017.

Brown A D, 1976. Microbial water stress, *Bacteriological Reviews*, 40(4), 803–846.

BS EN ISO, 2012. Corrosion of metals and alloys – Corrosivity of atmospheres – Guiding values for the corrosivity categories, BS EN ISO 9224:2012.

Burzan N, Lima R M, Frutschi M, Janowczyk A, Reddy B, Rance A, Diomidis N, Bernier-Latmani R, 2022. Growth and persistence of an aerobic microbial community in Wyoming bentonite MX-80 despite anoxic in situ conditions. *Frontiers in Microbiology*, 13.

Dueck A, Nilsson U, 2010. Thermo-Hydro-Mechanical properties of MX-80. Results from advanced laboratory tests. SKB TR-10-55, Svensk Kärnbränslehantering AB.

Gordon A, Pahverk H, Börjesson E, Johansson A J, 2018. Examination of copper corrosion specimens from ABM 45, package 5. SKB TR-18-17, Svensk Kärnbränslehantering AB.

Gordon A, Sjögren L, Taxén C, Johansson A J, 2017. Retrieval and post-test examination of packages 4 and 5 of the MiniCan field experiment. SKB TR-16-12, Svensk Kärnbränslehantering AB.

Greenspan L, 1977. Humidity fixed points of binary saturated aqueous solutions, *Journal of research of the national bureau of standards. A. Physics and Chemistry*, Vol. 81 A, No.1.

Han Q, Peng S, Xie Q, Wu Y, Zhang G, 2018. Iterative Reweighted Quantile Regression Using Augmented Lagrangian Optimization for Baseline Correction, 5th International Conference on Information Science and Control Engineering (ICISCE), Zhengzhou, 280–284.

Johansson A J, 2019. Corrosion of copper in repository-like field tests: compilation and analysis of data. SKBdoc 1713264 ver 1.0, Svensk Kärnbränslehantering AB.

Johansson A J, Svensson D, Gordon A, Pahverk H, Karlsson O, Brask J, Lundholm M, Malmström D, Gustavsson F, 2020. Corrosion of copper after 20 years exposure in the bentonite field tests LOT S2 and A3. SKB TR-20-14, Svensk Kärnbränslehantering AB.

Karnland O, Olsson S, Dueck A, Birgersson M, Nilsson U, Hernan-Håkansson T, Pedersen K, Nilsson S, Eriksen T, Rosborg B, 2009. Long term test of buffer material at the Äspö Hard Rock Laboratory, LOT project. Final report on the A2 test parcel. SKB TR-09-29, Svensk Kärnbränslehantering AB.

Karnland O, Olsson S, Sandén T, Fälth B, Jansson M, Eriksen T, Svärdström K, Rosborg B, Muurinen A, 2011. Long term test of buffer material at the Äspö HRL, LOT project. Final report on the A0 test parcel. SKB TR-09-31, Svensk Kärnbränslehantering AB.

King F, Robinson P, Watson C, Watson S, Metcalfe R, Burrow J, 2016. The atmospheric corrosion of stainless steel in stores (ACSIS) model, Amec Foster Wheeler report 17391-TR-010.

Liebsch G, Klimant I, Frank B, Holst G, Wolfbeis O S, 2000. Luminescence lifetime imaging of oxygen, pH, and carbon dioxide distribution using optical sensors. *Applied Spectroscopy*, 54(4).

Peng J, Peng S, Jiang A, Wei J, Li C, Tan J, 2010. Asymmetric least squares for multiple spectra baseline correction. *Analytica Chimica Acta*, 683, 63–68.

Pereira I A C, Ramos A R, Grein F, Marques M C, da Silva S M, Venceslau S S, 2011. A comparative genomic analysis of energy metabolism in sulfate reducing bacteria and archaea, *Frontiers in Microbiology*, 2.

- PreSens, 2024.** How does an oxygen sensor work? Precision Sensing. Available at: <https://www.prensens.de/support-services/faqs/question/how-does-an-oxygen-sensor-work-3> [8 July 2024].
- Rosborg B, Kosec T, Kranjc A, Pan J, Legat A, 2011.** Electrochemical impedance spectroscopy of pure copper exposed in bentonite under oxidic conditions. *Electrochimica Acta*, 56, 7862–7870.
- RS Components Ltd, 2023.** MSDS – RS-GCS-FLOSIL-600-V1 FLOWABLE SILICONE, Product code 187-3460.
- Smart N R, Adams R, 2006.** Natural analogues for expansion due to the anaerobic corrosion of ferrous metals. SKB TR-06-44, Svensk Kärnbränslehantering AB.
- Smart N R, Rance A P, 2009.** Miniature canister corrosion experiment – results of operations to May 2008. SKB TR-09-20, Svensk Kärnbränslehantering AB.
- Smart N R, Rance A P, Reddy B, Fennell P A H, Winsley R J, 2012.** Analysis of SKB MiniCan Experiment 3. SKB TR-12-09, Svensk Kärnbränslehantering AB.
- Smart N R, Rose S R, Nixon D J, Rance A P, 2013.** Metallographic Analysis of SKB MiniCan Experiment 3. SKB R-13-35, Svensk Kärnbränslehantering AB.
- Taxén C, 2013.** Ytprofiler på kopparkapslar från deponeringshål 5 och 6 i försöksserien Prototyp. SKB P-13-50, Svensk Kärnbränslehantering AB (In Swedish.)
- Taxén C, Lundholm M, Persson D, Jakobsson D, Sedlakova M, Randelius M, Karlsson O, Rydgren P, 2012.** Analyser av koppar från prototypkapsel 5 och 6. SKB P-12-22, Svensk Kärnbränslehantering AB (In Swedish.)
- Vikman M, Matusiewicz M, Sohlberg E, Miettinen H, Tiljander M, Järvinen J, Itälä A, Rajala P, Raulio M, Itävaara M, Muurinen A, Olin M, 2018.** Long-term experiment with compacted bentonite, VTT Technology 332.
- Wendel E, Gordon G, Börjesson E, Wärnheim A, Bergendal E, Johansson J, Svensson D, 2022.** Analysis of corrosion products on filter housings in the Lasgit field experiment. SKB TR-22-01, Svensk Kärnbränslehantering AB.
- Wersin P, 2013.** LOT A2 test parcel. Compilation of copper data in the LOT A2 test parcel. SKB TR-13-17, Svensk Kärnbränslehantering AB.
- Åkesson M, Laitinen H, 2022.** Gas phase composition during the unsaturated period. Status report June 2022, SKBdoc 1983850 ver 1.0, Svensk Kärnbränslehantering AB.

Additional information

Table A-1. Images of the pristine copper coupons included in the small glass cells. Layer 1 is at the top of the stainless steel sample holder and Layer 6 is at the bottom.

	S1	S2	S3
Layer 1			
Layer 2			
Layer 3			
Layer 4			
Layer 5			
Layer 6			

Table A-2. Images of the pristine copper coupons included in the medium glass cells. Layer 1 is at the top of the stainless steel sample holder and Layer 6 is at the bottom.

	M1	M2	M3
Layer 1			
Layer 2			
Layer 3			
Layer 4			
Layer 5			
Layer 6			

Table A-3. Images of the pristine copper coupons included in the large glass cells. Layer 1 is at the top of the stainless steel sample holder and Layer 6 is at the bottom.

	L1	L2	L3
Layer 1			
Layer 2			
Layer 3			
Layer 4			
Layer 5			
Layer 6			

Table A-4. Images of the pristine copper coupons included in the time zero (t_0) glass cell. Layer 1 is at the top of the stainless steel sample holder and Layer 6 is at the bottom.

	t_0
Layer 1	
Layer 2	
Layer 3	
Layer 4	
Layer 5	
Layer 6	

Table A-5. Matrix of glass cells. Cell nomenclature is highlighted in bold text.

Cell type	Environment	Air volumes of all cells	Number of cells set up	Cells tipped during project	Cells disassembled	Cells remaining
Experimental cells	6 × copper coupons + bentonite (S# , M# , L#)	Volume 1 ~0.20 L (S#)	3	S2 & S3	S3	S1 & S2
		Volume 2 ~0.40 L (M#)	3	M2	M1 & M3	M2
		Volume 3 ~0.75 L (L#)	3	-	L1 & L2	L3
Control cells	Bentonite (no copper coupons) (C#)	Volume 1 ~0.20 L	3	C1	-	C1, C2 & C3
	Stainless steel holder only (no bentonite) (SS)	Volume 1 ~0.20 L	1	-	-	SS
	6 × copper coupons + bentonite (t₀)	N/A	1	N/A	t ₀	-

Table A-6. Average weight for each coupon in the glass cells. Coupon 6 is at the bottom and coupon 1 is at the top.

Glass cell	Coupon 1 (g)	Coupon 2 (g)	Coupon 3 (g)	Coupon 4 (g)	Coupon 5 (g)	Coupon 6 (g)
S1	2.94738	2.99251	3.01666	3.00554	2.98648	2.94776
S2	3.03242	2.97475	2.98313	2.97545	2.99231	2.95100
S3	3.02765	2.98489	3.02533	2.96717	2.98440	2.96184
M1	2.98630	2.96580	2.99651	2.99145	2.98163	2.94506
M2	2.99523	2.99851	3.03293	2.97069	2.95031	2.94400
M3	2.98142	2.97876	2.94820	2.97427	3.03541	2.95828
L1	2.98862	2.97210	2.93909	2.93222	2.97869	3.00180
L2	2.98169	2.98138	2.98056	3.01756	3.02152	2.95970
L3	2.99121	3.02089	2.94879	2.99469	2.93184	3.00279
t ₀	2.99474	2.98386	2.94508	2.97362	2.97748	3.00610

Table A-7. Mass of bentonite used in the individual layers of each glass cell stainless steel sample holder. The mass of bentonite in layer 7 is greater due to the lack of a coupon in that layer. Layer 7 is at the bottom of the sample holder and layer 1 is at the top.

Glass cell	Layer 1 (g)	Layer 2 (g)	Layer 3 (g)	Layer 4 (g)	Layer 5 (g)	Layer 6 (g)	Layer 7 (g)
S1	2.8	3.1	3.1	3.1	3.1	3.1	4.0
S2	2.8	3.1	3.1	3.1	3.1	3.1	4.0
S3	2.8	3.1	3.1	3.1	3.1	3.1	4.0
M1	2.8	3.1	3.1	3.1	3.1	3.1	4.0
M2	2.8	3.1	3.1	3.1	3.1	3.1	4.0
M3	2.8	3.1	3.1	3.1	3.1	3.1	4.0
L1	2.8	3.1	3.1	3.1	3.1	3.1	4.0
L2	2.8	3.1	3.1	3.1	3.1	3.1	4.0
L3	2.8	3.1	3.1	3.1	3.1	3.1	4.0
C1	3.0	3.8	3.8	3.8	3.8	3.8	4.6
C2	3.0	3.8	3.8	3.8	3.8	3.8	4.6
C3	3.0	3.8	3.8	3.8	3.8	3.8	4.6

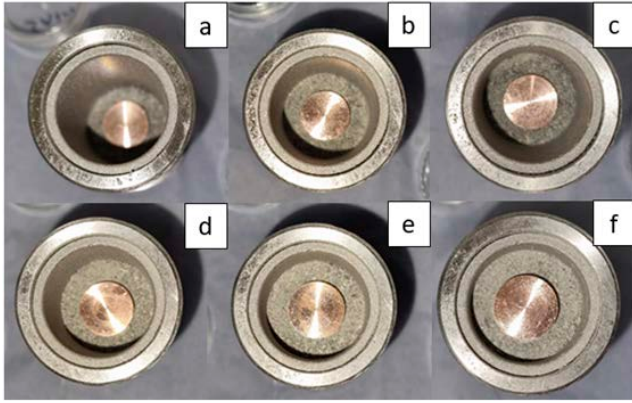


Figure A-1. Image of each coupon during the assembly of the S1 sample holder: a, layer 6; b, layer 5; c, layer 4; d, layer 3; e, layer 2; f, layer 1.

Estimated uncertainty of corrosion rate measurements

The resolution of the individual measurements used in the mass loss procedure are described in Table A-8. Table A-9 shows the estimated range of measurement uncertainty for the corrosion rate measurements determined using the mass loss technique. The magnitude of the uncertainty of the corrosion rate is a function of the corrosion rate itself. Hence, the measurement uncertainty has been quoted for the highest and lowest corrosion rate observed in any of the test conditions.

Table A-8. Resolution of the measurements used in the calculation of corrosion rates as determined by mass loss.

Measurement	Resolution
Mass	± 5 µg
Dimensions	± 0.5 mm
Exposure duration	± 8 hours
Density (of pure copper)	± 0.05 g cm ⁻³

Table A-9. Estimated corrosion rate measurement uncertainty calculated based on the highest and lowest observed corrosion rates.

Uncertainty (highest/lowest)	Calculated Uncertainty of Corrosion rate (µm yr ⁻¹) for K=1 (66 % coverage)	Calculated Uncertainty of Corrosion rate (µm yr ⁻¹) for K=2 (95 % coverage)
Small cell (251 days)	0.045	0.090
Large cells (251 days)	0.062	0.123
T ₀ (251 days)	0.050	0.101
Medium cells (614 days)	0.023	0.046

SKB is responsible for managing spent nuclear fuel and radioactive waste produced by the Swedish nuclear power plants such that man and the environment are protected in the near and distant future.

skb.se